Agarose disk electroporation method for *ex vivo* retinal tissue cultured at the air-liquid interface reveals electrical stimulus-induced cell cycle reentry in retinal cells

Megan L. Stone[1], Hannah H. Lee[2] , Edward M. Levine[1,2,*]

[1]Department of Cell and Developmental Biology
Vanderbilt University, Nashville TN 37232

[2]Department of Ophthalmology and Visual Sciences
Vanderbilt University Medical Center, Nashville TN 37232

*Corresponding author
Ed.levine@vumc.org

Keywords:

Ethics statement: All procedures and experiments with mice were approved under protocol M1600035 by the Vanderbilt Institutional Animal Care and Use Committee and conformed to the ARVO guidelines for the use of animals in vision research. The research was conducted in concordance with the NIH guidelines for Responsible Conduct in Research (RCR).

The authors declare no conflicts of interest

Motivation

Tissues cultured at the air-liquid interface, such as retinal tissue, are adhered to a filter membrane with media underneath but not fully submerged. If tissues are fully submerged in liquid, they detach from the membrane and become damaged. Electroporation typically requires tissue submergence for electric current flow. We have developed a submergence-free electroporation method using an agarose disk for electric current delivery that can efficiently and consistently electroporate *ex vivo* retinal tissue cultured at an air-liquid interface without the need to submerge the tissue and disrupt the culture system.

Summary

It is advantageous to culture the *ex vivo* murine retina along with many other tissue types at the air-liquid interface. However, gene delivery to these cultures can be challenging. Electroporation is a fast and robust method of gene delivery, but typically requires submergence in a liquid buffer to allow electric current flow. We have developed a submergence-free electroporation technique using that allows for efficient gene delivery to the *ex vivo* murine retina. This method advances our ability to use *ex vivo* retinal tissue for genetic studies and can easily be adapted for any tissue cultured at an air-liquid interface. Use of this method has revealed valuable insights on the state of *ex vivo* retinal tissues and the effects of electrical stimulation on retinal cells.

Introduction

The retina is a highly structured organ that relies on intercellular communication to respond to injury and maintain homeostasis[1–3]. The field of retinal research relies on various model systems to study the structure, function, and pathology of the retina. *Ex vivo* explant systems involve isolating and culturing tissue samples, which allows for the preservation of the complex structure and physiological characteristics of organs like the retina[4–6]. *Ex vivo* retinal tissue cultures offer several advantages over other models, particularly in the study of retinal function and degeneration. *Ex vivo* models allow the study of cellular changes within the context of the tissue structure compared to *in vitro,* which lack the 3-dimensional context, or organoid models, which lack prior organismal physiological integration and external environmental exposures. Furthermore, *ex vivo* models provide the opportunity for more advanced manipulations and analyses that may be difficult to perform and interpret *in vivo*, such as live imaging, small molecule delivery and cell reprogramming studies[7,8].

Ex vivo retinal tissues experience cell death and activation of Müller glia over time in culture. This makes *ex vivo* retinal explant models particularly valuable as an injury model[6,9–12]. It is of interest to improve the health of these cultures to study the retina under normal physiological conditions, however. Innovations in culture technique and supplementation has been shown to promote the survival of *ex vivo* retinal explants. One such innovation is to culture tissue on PTFE or polycarbonate membrane inserts with media below the membrane filter. This technique maintains an air-liquid interface that is valuable for gas exchange in the tissue[9,13,14]. Lung, liver, skin and brain tissue are commonly cultured at the air-liquid interface and the methods described here could be adapted for use with these tissues[15–19]. Optimization studies to preserve the

46 health of *ex vivo* retinas are ongoing, but as is, long term culture of *ex vivo* retinal tissue
47 is a useful injury context to observe live changes in response to genetic manipulation.

48 Gene delivery to *ex vivo* retinal tissue can be challenging. Viral methods, such as
49 AAV and lentivirus, are limited by size constraints for DNA cargo and have delayed
50 expression time compared to non-viral methods[20,21]. Electroporation is a robust method
51 for plasmid delivery that promotes quick expression[22–24]. However, electroporation
52 requires that cells or tissues be submerged in buffer with an electrode to allow electric
53 current flow and that direct contact between the tissue and electrodes is avoided.
54 Submersion of tissue is feasible prior to culture, but submerging tissues at the air-liquid
55 interface causes detachment from the support membrane, which restricts the ability to
56 transfect after cultures are established.

57 To overcome the obstacles to delivery of genetic material to *ex vivo* retinal
58 tissues, we developed an electroporation method that avoids tissue submergence in a
59 large volume and prevents direct contact with the electrode by generating a confined
60 liquid interface between the electrode and sample (Figure 1). With this adaptation, we
61 characterized the efficiency of electroporation at 1- and 14-days *ex vivo* (DEV) in the
62 air-liquid interface culture format. We also characterized the effects of electrical
63 stimulation on cell proliferation in *ex vivo* retinal cultures to provide clarity to
64 investigators that may use this method in future studies that the effects of
65 electroporation are not inert in the *ex vivo* retinal system. Lastly, we demonstrate the
66 limitations in assessing transfection efficiency when relying on a fluorescent reporter
67 construct as a readout.
68

Results

Agarose disk electroporation of *ex vivo* retinal tissue efficiently delivers genetic material with minimal tissue submergence

The components required for this electroporation system are: (1) an arm electrode that can be fixed to a ring stand and lowered onto cultured retinas in cell culture insert, (2) a 0.5% agarose disk, 5mm thick and the width of the arm electrode, (3) DNA with an electroporation dye containing glycerol to increase viscosity, and (4) an anode dish; aluminum foil at the bottom of a 100mm petri dish, underneath the tissue. Electroporation was performed at 24 hours (1DEV), or 14 days (14DEV) and retinas were fixed at 72-96 hours post-electroporation. All *ex vivo* retinas were dissected from mice between 8-12 weeks of age.

Prior to the experiment, 500uL of 0.5% liquified agarose (RPI, A20090) is pipetted into 1 well of a 24-well plate (Corning, CLS3527) and set aside for 30 minutes in a sterile culture hood. A disk roughly 10 mm wide is created from the solidified agarose using the end of a plastic transfer pipet (Fisherbrand 13-711-7M), cut above the tapered tip, to stamp a disk shape. The agarose disk is then adhered to the arm electrode (Bulldog Bio, CUY700P7L) surface (Figure 1C) while the arm electrode is suspended face up using a micromanipulator (Narishige, UMM-3C). The disk should be adhered with no air bubbles formed between it and the electrode, which could impede electrical flow. Once the agarose disk is adhered to the electrode, 10-15uL of DNA-glycerol mixture (1-3 pMol DNA, 2.5% methyl green dye (MCE, HYD0163) and 7.5% glycerol (Sigma Aldrich, G7893) is pipetted on top of the agarose disk facing upward (Figure 1C, D). To complete the electric circuit, chilled PBS (Corning, 21-040-CV) (4°C) is placed on the anode surface and the cell culture insert (Millicell, PIC0RG50)

containing the retinal tissue is placed on top (Figure 1A, B). The arm electrode with the agarose disk and DNA mixture is rotated 180 degrees and the DNA mixture will stay adhered to the agarose as a suspended drop. The arm electrode is lowered until the DNA mixture contacts the tissue, at which point current is delivered in five 50ms square wave pulses (25V) with 250ms intervals between pulses (Figure 1E). Fluorescent reporter-expressing plasmids with a general promoter, such as pCMV-eGFP, were used to assess transfection.

Differences in cell types transfected at the edge and center of the tissue at 1DEV

Since retinas were cultured with their basal surface toward the air-liquid interface, the cells most accessible to plasmid uptake were astrocytes, retinal ganglion cells, displaced amacrine cells, and Müller glia[25,26]. Electroporation (referred to as transfection hereon) of pCMV-eGFP at 1DEV revealed a consistent difference in morphology from cells transfected at the center of the retina compared to the edge that is defined as 100µm in from tissue periphery around perimeter (Figure 2B). Cells transfected at the edge of the tissue resembled Müller glia in morphology (Figure 2D, G). Colocalization of eGFP with SOX9, a marker of Müller glia[27–29], is consistent with this observation (Figure 2D). In contrast, transfected cells toward the center of the tissue had a retinal ganglion cell-like morphology, which is distinctly recognizable by long axons converging at the optic nerve head (Figure 2C, F). Transfection of pCMV-mCherry[30] into retinas from Thy1:YFP-16 mice (Thy1:YFP), which express YFP in a large cohort of RGCs in addition to other inner retinal neurons[31], provided further evidence that RGCs were transfected (Figure 2G). Quantifications revealed that the distributions of transfected

117 cells were skewed toward SOX9+ cells at the tissue edge and toward Thy1:YFP+ cells
118 toward the center (Figure 2H). Overall, there is equivalent efficiency in transfection of
119 Müller glia and Thy1:YFP+ cells in retinas transfected at 1DEV, but their distribution is
120 location-dependent (Figure 2H).
121
122 **Müller glia are preferentially transfected at 14DEV**
123 Changes in cell survival, location, size, and morphology occur over time in
124 culture[10–12]. Retinal tissue was electroporated at 14DEV to assess differences in
125 transfection profile over time. Cells transfected at the edge of tissue resembled Müller
126 glial morphology (Figure 3D, G), but the characteristic retinal ganglion cell morphology
127 visible in the center in retinas transfected at 1DEV was not observed (Figure 3C, D, F,
128 G). Staining for SOX9 revealed an increase in transfected Müller glia compared to inner
129 retinal neurons as assessed with Thy1:YFP regardless of location (Figure 3D, G).
130 These observations suggest that there is a decrease in neurons transfected at 14DEV
131 overall, and an increase in transfection of Müller glia at the tissue center (Figure 3H).
132 To visualize tissue structure with respect to inner neurons and Müller glia at 1
133 and 14DEV, orthogonal slice projections were constructed from Z-stack confocal
134 images of untransfected Thy1:YFP or Rlbp1:eGFP transgenic retinas, the latter serving
135 as a reporter for Müller glia[32]. An ROI "slice" was cropped from each image in the same
136 orientation to observe center and edge regions (Figure 4). At 1DEV, YFP+ cells were
137 observed in the ganglion cell layer (GCL) and inner nuclear layer (INL; Figure 4A).
138 Fluorescence was also observed in the inner plexiform layer (IPL), suggesting
139 maintained laminar organization. However, fewer YFP+ cells were observed in the GCL

140 at the retinal edge (Figure 4A, left). At 14DEV, YFP expression in the GCL was
141 diminished in the central region but interestingly was retained in the IPL and INL (Figure
142 4B). In Rlbp1:eGFP tissue, GFP expression was also detectable in the GCL at the
143 center of tissue at 1DEV (Figure 4C), consistent with their radial morphology[33]. At
144 14DEV, there was an increase in GFP expression relative to the total tissue volume
145 including at the basal surface of the retina, where plasmids are placed for
146 electroporation (Figure 4D). This could be due to Müller glia survival, proliferation,
147 hypertrophy, altered morphology, or increased GFP expression on a per cell basis,
148 none of which are mutually exclusive. Importantly, the loss of RGCs and accumulation
149 of Müller glia at the basal surface could explain the shift toward preferential transfection
150 of Müller glia at 14DEV.
151

152 **Electrical stimulation induces BrdU incorporation in *ex vivo* retina**

153 The adult mouse retina is normally quiescent, but proliferation can occur to a
154 limited extent in non-neuronal cells such as microglia and Müller glia in response to
155 injury and/or inflammation, two contexts that are likely occurring in the *ex vivo* retina
156 [6,10,12,34–39]. Proliferation has also been shown to increase in response to electrical
157 stimulation[40–44], though this has yet to be shown in the retina. We therefore assessed
158 proliferation in the cultures with and without electrical stimulation. Electrical stimulation
159 was delivered using the electroporator with the same settings for transfection and three
160 conditions were tested: no electroporation (-*EP*), electroporation with DNA loading
161 solution lacking DNA (+*EP*), or electroporation with pCMV-eGFP plasmid (+EP^{DNA}).
162 These treatments were applied to *ex vivo* retinas at 1DEV or 14DEV. At 72 hours post-

163 treatment,16uM BrdU was delivered in the cell culture media for 24 hours to assess cell
164 cycle reentry that persists beyond the initial response to electrical stimulation (Figure
165 5A). At both times in culture, there were significant increases in BrdU+ cells per mm^3 in
166 the +*EP* and +EP^{DNA} conditions compared to the -*EP* condition (Figure 5B,C). Similar
167 levels of BrdU incorporation in the +*EP* and +EP^{DNA} conditions were anticipated since
168 eGFP expression is not expected to promote proliferation. The increase in proliferation
169 observed in +*EP* and +EP^{DNA} conditions compared to the -*EP* condition revealed that
170 electrical stimulation of retinal tissue *ex vivo* can lead to changes in cell behavior
171 associated with cell cycle activity.
172

173 **The proportion of BrdU+ cells that are Müller glia increases in 14DEV compared**
174 **to 1DEV retinas and following electrical stimulus**

175 We predicted that microglia and Müller glia were re-entering the cell cycle in
176 response to electrical stimulation. To assess this, *ex vivo* retinas were immunostained
177 with the microglial marker IBA1 or with SOX9 in combination with BrdU detection, and
178 colocalization with BrdU was quantified to determine the number of these cells
179 undergoing cell cycle entry (Figure 6). In retinas treated at 1DEV or 14DEV, BrdU+
180 microglia and Müller glia were observed in -*EP* and +*EP* conditions (Figure 6A, B).
181 Quantification revealed a significantly increased proportion of BrdU+ Müller glia,
182 indicated by SOX9 labeling, in retinas treated at 14DEV in +*EP* retinas compared to
183 1DEV +*EP* (Figure 6C). The number of BrdU+ Müller glia significantly increased in +*EP*
184 retinas treated at 14DEV compared to 1DEV +*EP* retinas and 14DEV -*EP* retinas,
185 whereas the number of BrdU+ microglia remained steady (Figure 6D). These results

186 suggest an increase in cell cycle entry in Müller glia that correlates with time in culture
187 and electrical stimulation.
188
189 **Transfection of pCMV-Cre reveals a higher transfection efficiency than pCMV-**
190 **eGFP**
191 A limitation of using fluorescent reporter expression constructs such as pCMV-
192 eGFP is that cells could have been transfected but expression of the fluorescent protein
193 was below detection. Since as few as 4 molecules of Cre recombinase are sufficient for
194 recombination[45–47], we predicted that transfection of a construct expressing Cre under
195 the control of the same promoter/enhancer elements (pCMV-Cre) would reveal a higher
196 transfection efficiency than what can be detected with pCMV-eGFP (Figure 7A). To test
197 this, pCMV-Cre[48] and pCMV-eGFP were co-transfected at equimolar concentrations
198 into *ex vivo* retinas from *Rosa*^{AI14} mice, which express tdTom after Cre recombination.
199 *Ex vivo* retinas were analyzed 5 days after transfection at 1DEV or 14DEV.
200 As expected, we observed similar expression patterns of eGFP and tdTom in co-
201 transfected retinas, regardless of location in the tissue or days in culture (Figure 7B, C).
202 Cell quantification revealed that the majority of eGFP+ cells expressed tdTom, but this
203 was not the case for tdTom+ cells, of which the minority were GFP+ (Figure 7D).
204 Consistent with this, tdTom+ cells constituted a higher proportion of the transfected
205 population than eGFP+ cells (Figure 7E; Table S1). While several factors such as
206 plasmid size, nucleic acid composition, or secondary structures could affect transfection
207 efficiency, we expected the expression characteristics of these constructs to be similar
208 since they are similar in size and share the same promoter and enhancer elements. In

209 this context, these data suggest that the transfection efficiency is greater than what can
210 be observed by transfection of expression plasmids for fluorescent proteins.
211
212 **pCMV-Cre exhibited the highest transfection efficiency when compared to other**
213 **Cre-expression constructs**

214 The CMV promoter is considered a cell ubiquitous promoter. However, studies
215 have shown that CMV promoters are not expressed well in post-mitotic neurons
216 compared to other cell types[49,50] which could reduce the apparent transfection efficiency
217 of CMV-based expression vectors in *ex vivo* retinal cultures. To address this, we tested
218 two constructs where Cre is driven by distinct regulatory elements: pCAG-Cre which
219 contains the promoter for the chicken *beta-Actin* gene and CMV immediate-early
220 enhancer[22], and pBS513 EF1alpha-Cre (pEf1α-Cre), which contains the promoter
221 region of the *Elongation Factor 1 alpha* gene[51]. In each case, pCMV-eGFP was co-
222 transfected at equimolar concentrations. pCAG-Cre and pEf1α-Cre activated tdTom
223 expression and the expression patterns of tdTom overlapped with eGFP (Figure 8A, D).
224 Cell quantification of retinas co-transfected at 1DEV with pCAG-Cre and pCMV-eGFP
225 revealed similar proportions of eGFP+ cells expressing tdTom and tdTom+ cells
226 expressing eGFP (Figure 8B, left), whereas in retinas transfected at 14DEV, the
227 proportion of eGFP+ cells expressing tdTom was greater than tdTom+ cells expressing
228 eGFP (Figure 8B, right). At both timepoints, tdTom+ cells constituted a higher proportion
229 of the entire transfected cell population (Figure 8C). These data suggest pCAG-Cre
230 behaves similarly to pCMV-Cre.

231 Like pCAG-Cre, retinas co-transfected at 1DEV with pEF1α-Cre and pCMV-
232 eGFP had similar proportions of eGFP+ cells expressing tdTom and tdTom+ cells
233 expressing eGFP (Figure 8E, left). In contrast to pCAG-Cre, the proportion of tdTom+
234 cells expressing eGFP was greater than eGFP+ cells expressing tdTom in retinas
235 transfected at 14DEV (Figure 8E, right). These patterns were also reflected in the
236 relative proportions of eGFP+ or tdTom+ cells that comprise the transfected cell
237 population (Figure 8F).

238 Next, we compared the transfection efficiencies of pCMV-Cre, pCAG-Cre, and
239 pEF1α-Cre. Since pCMV-eGFP was co-transfected with each construct in equimolar
240 quantities, we calculated the ratios of tdTom+ cells to eGFP+ cells in the co-transfected
241 retinas to compare the relative transfection efficiencies of the three Cre expression
242 constructs. In retinas transfected at 1DEV, pCMV-Cre was most efficient at activating
243 tdTom expression, as revealed by a ratio of 2.4 tdTom+ cells per eGFP+ cell and
244 compared to pCAG-Cre at 1.5 tdTom+ cells per eGFP+ cell, and pEF1α-Cre at 1.1
245 tdTom+ cells per eGFP+ cell (Figure 8G, left; Table S1). At 14DEV, the efficiencies
246 pCMV-Cre and pCAG-Cre were similar as revealed by ratios of 1.6 and 1.7 tdTom+
247 cells per eGFP+ cell, respectively. pEF1α-Cre was the least efficient at activating tdTom
248 expression as indicated by a ratio of 1.1 eGFP+ cells per tdTom+ cell (Figure 8G, right).
249 These results indicate that all three expression constructs can drive Cre expression in
250 the *ex vivo* retina, but CMV regulatory elements are more efficient than the EF1α
251 promoter. A comparison of the distributions of transfected cells expressing eGFP,
252 tdTom, or both, for each construct supports this conclusion (Figure S1; Table S1).

253

Discussion

This study introduces a novel method of electroporation for *ex vivo* retinal tissue cultured at the air-liquid interface that avoids submergence of the tissue or direct contact with the electrode. This electroporation method offers a rapid and time-dependent transfection efficiency while maintaining tissue integrity. This method is cost effective and does not require specialized equipment, making it generally accessible. Though we have only tested retinal tissue, it could easily be adapted for any tissue type that is cultured using an air liquid interface method, including lung, intestine, or skin[13,14,52,53].

We observed a difference in the cell types transfected at different times in culture. This finding suggests that the timing of the transfection is useful for targeting specific cell populations within the retina. Müller glia undergo hypertrophy and migration in response to injury signals from retinal neurons[54–58]. Likely, the increase in availability of Müller glia at the electroporation surface is due to the loss of retinal ganglion cells and changes in Müller glial morphology associated with tissue remodeling[59].

We found that the application of electrical stimulus alone leads to an increase in proliferation in Müller glia as indicated by BrdU incorporation. The mammalian retina is quiescent after retinal development, but Müller glia and microglia are known to exhibit limited proliferation in response to injury or inflammation. This proliferation occurs typically in young postmitotic mice and diminishes after injury onset[6,10,12,34–36,39,55,58]. Postmitotic Müller glia have been shown to proliferate in culture, however this effect was observed in *ex vivo* retinas from P10 mice and diminished by P14[10]. The mice used here were adults between 8-12 weeks of age.

277 Proliferation resulting from electrical stimulation has been reported in multiple cell
278 types, including neural stem cells, human embryonic stem cells, osteoblasts, and
279 fibroblasts[40,64–67]. Electroporation can also stimulate neural progenitor cell differentiation
280 into neurons[67–69]. Amongst the BrdU+ cell population, there was a significant increase in
281 BrdU+ Müller glia at 14DEV and following electrical stimulus whereas the presence of
282 BrdU+ microglia was not dependent on time in culture. This could indicate an increase
283 in Müller glia in the tissue at 14DEV or a change in cell state that leads to increased
284 proliferation of Müller glia. Further studies are needed to determine whether proliferating
285 Müller glia in this context also acquire neurogenic properties.

286 Delivery of a Cre expression construct into a recombination reporter mouse strain
287 predicts that true transfection efficiency is greater than observed with a fluorescent
288 reporter expression construct, meaning more cells may receive gene delivery than
289 accounted for. It is advantageous with this system to use a sensitive reporter for
290 electroporation, like Cre-mediated reporter expression, or to boost the signal for the
291 fluorescent reporter with antibodies to enhance detection when analyzing fixed tissue.

292 Clinical studies indicate that low current electrical stimulation to the eye leads to
293 better outcomes in patients with retinal dystrophies[60,61]. *In vitro* studies in Müller glia
294 isolated from the dissociated mouse retina show that electrical stimulation increases
295 expression of neurotropic factors and retinal progenitor markers, leading to an increase
296 in proliferation[62,63]. The effect of electrical stimulation on Müller glia in the intact mouse
297 retina has not been shown. This indicates a change in cell behavior following electrical
298 stimulus that is not typical under normal physiological conditions.

299

300 **Limitations of Study**

301 While this study provides valuable insights into the overall efficiency of
302 transfection, especially on some retinal cell types, further research is necessary to fully
303 characterize the effects on every cell type. This method has only been tested on retinal
304 tissue, though it could be adapted for other tissue types cultured in an air-liquid interface
305 format. Proliferation observed in this study was measured using BrdU incorporation,
306 which labeled cells during S-phase of mitosis. BrdU could incorporate in cells that are
307 then arrested in S-phase and do not fully divide. Further testing is required to
308 understand the extent of proliferation following electrical stimulation.

309 Although certain cell types may be more amenable to electroporation, the
310 method is not inherently cell type specific. Other methods of transfection should be
311 employed if a study requires expression to only occur in certain cell types. We
312 demonstrated that BrdU incorporation is induced following electrical stimulation with this
313 method. Based on this finding, it is important that studies that use electroporation to the
314 *ex vivo* retina as a gene delivery method include electrical stimulation without DNA in
315 addition to other transfection controls to distinguish the effects of electrical stimulation
316 and genetic manipulation when assessing proliferation.

317 Comparisons of pCAG-Cre and pEF1α-Cre in this study do not account for
318 variability in cell type-specific preferential transfection. It is outside the scope of this
319 study to delineate cell type preferential transfection with these constructs but is worthy
320 of investigation by those interested in using this method to target specific retinal cell
321 types.

Acknowledgments

Funding for this study was provided by the National Eye Institute (R01-EY013760; P30-EY008126), the Janet and Jim Ayers Research Fund in Regenerative Visual Science, the William A. Black Chair in Ophthalmology, and an unrestricted grant from Research to Prevent Blindness, Inc. M.L.S was supported by the Vanderbilt Vision Training Grant (T32-EY007135) and a Ruth L. Kirschstein Predoctoral Individual National Research Service Award (F31EY035554) from the National Eye Institute. Confocal imaging and Imaris software analysis were performed at the Vanderbilt Cell Imaging and Shared Resource. The Zeiss LSM710 confocal microscope used for this study was acquired with funding from NIH (S10-RR027396). We thank Zachary Sanchez for assistance in photographing the electroporation set up and to members of the Levine and Fuhrmann laboratories for their insights and feedback.

Author Contributions

Conceptualization, E.M.L and M.L.S; Methodology E.M.L, H.H.L, and M.L.S; Formal Analysis, M.L.S; Investigation, M.L.S; Resources, E.M.L; Data Curation, M.L.S; Writing (original draft), M.L.S; Writing (review & editing), M.L.S, H.L., E.M.L; Visualization, M.L.S; Supervision, E.M.L; Project Administration, E.M.L; Funding Acquisition, E.M.L.

Declaration of Interests

The authors declare no competing interests.

Figure Legends

Figure 1. Visual methodology of agarose disk electroporation for *ex vivo* retinas.

(A) Murine retinal tissue cultured at the air-liquid interface on PFTE membrane after 5 days *ex vivo* (5 DEV) (1X, brightfield). (B) Agarose disk electroporation set-up. 5mm high, 10mm diameter 0.5% agarose disk adhered to an arm electrode above an anode dish containing *ex vivo* retinal tissue on PTFE membrane with chilled PBS underneath. (C) 12uL of DNA-glycerol mixture is pipetted onto the agarose disk facing upward. (D) DNA-Glycerol mixture on top of agarose disk facing upward. (E) 180° rotation electrode

353 arm containing agarose disk and DNA-glycerol mixture lowered onto *ex vivo* retinal
354 tissue.
355
356 **Figure 2. Preferential transfection at 1DEV of Müller glia and neurons at the edge**
357 **and center of tissue, respectively.** (A) Timeline of experimental design for 1DEV
358 transfection of wild type tissue with pCMV-eGFP reporter plasmid and staining for SOX9
359 to detect Müller glia. (B) Schematic indicating edge (100μm from the retina periphery)
360 and center of tissue. (C) pCMV-eGFP transfected cells in wild-type tissue transfected at
361 1DEV. Scale bar: Left, 200μm. Right, 50μm. (D) Left: pCMV-eGFP transfected cells,
362 middle: SOX9 staining, and right: overlap of eGFP and SOX9 at the center (top) and
363 edge (bottom) of tissue at 1DEV. Arrows indicate double-labeled cells. Scale Bar:
364 50μm.(E) Timeline of experimental design for 1DEV transfection of Thy1:YFP neuronal
365 reporter tissue with pCMV-mCherry reporter plasmid. (F) pCMV-mCherry transfected
366 cells in Thy1:YFP tissue transfected at 1DEV (YFP not shown). Scale bar: Left, 200μm,
367 Right, 50μm. (G) Left: pCMV-mCherry transfected cells, middle: Thy1:YFP reporter, and
368 right: overlap of mCherry and YFP at the center (top) and edge (bottom) of tissue after
369 electroporation at 1DEV. Arrows indicate double-labeled cells. Scale Bar: 50μm. (H)
370 Quantification of percentage of cells transfected with pCMV-eGFP that are SOX9+ and
371 cells transfected with pCMV-mCherry that are Thy1:YFP+ at the edge, center and
372 combined edge and center of tissue after electroporation at 1DEV. Mean ± SEM is
373 shown. N=4-6. *$p < 0.05$, **$p < 0.01$, ***$p < 0.001$, ****$p < 0.0001$. No bracket indicates p
374 > 0.05. All statistical tests performed on arcsine transformed values.
375

376 **Figure 3. Preferential transfection of Müller glia at 14DEV.** (A) Timeline of
377 experimental design for 14DEV transfection of wild type tissue with pCMV-eGFP
378 reporter plasmid and staining for SOX9 to detect Müller glia. (B) Schematic indicating
379 edge (100μm from the retina periphery) and center of tissue. (C) pCMV-eGFP
380 transfected cells in wild-type tissue transfected at 14DEV. Scale bar: Left, 200μm. Right,
381 50μm.(D) Left: pCMV-eGFP transfected cells, middle: SOX9 staining, and right: overlap
382 of eGFP and SOX9 at the center (top) and edge (bottom) of tissue at 14DEV. Arrows
383 indicate double-labeled cells. Scale Bar: 50μm. (E) Timeline of experimental design for
384 14DEV transfection of Thy1:YFP neuronal reporter tissue with pCMV-mCherry reporter
385 plasmid. (F) pCMV-mCherry transfected cells in Thy1:YFP tissue transfected at 14DEV
386 (YFP not shown). Scale bar: Left 200μm, Right, 50μm. (G) Left: pCMV-mCherry
387 transfected cells, middle: Thy1:YFP reporter, and right: overlap of mCherry and YFP at
388 the center (top) and edge (bottom) of tissue after electroporation at 14DEV. Arrows
389 indicate double-labeled cells. Scale Bar: 50μm. (H) Quantification of percentage of cells
390 transfected with pCMV-eGFP that are SOX9+ and cells transfected with pCMV-mCherry
391 that are Thy1:YFP+ at the edge, center and combined edge and center of tissue after
392 electroporation at 14DEV. Mean ± SEM is shown. N=4-5. *$p < 0.05$, **$p < 0.01$, ***$p <$
393 0.001, ****$p < 0.0001$. No bracket indicates $p > 0.05$. All statistical tests performed on
394 arcsine transformed values.
395
396 **Figure 4. Changes in tissue structure at electroporation surface in orthogonal**
397 **slice projections of 1DEV & 14DEV Thy:YFP and Rlbp1:eGFP retinas favor**
398 **electroporation of Müller glia at 14DEV.** Orthogonal slice projections of center and

edge created from 3D projections of ROIs (354.25 pixels by 11.76 pixels) to visualize cross sections within *ex vivo* retinas from transgenic mouse models. ONL: Outer nuclear layer. INL: Inner nuclear layer. GCL: Ganglion cell layer. IPL: Inner plexiform layer. * denotes the optic nerve head (ONH). (A) Orthogonal slice projections of the edge (left) and center (right) of Thy1:YFP *ex vivo* tissue fixed at 1DEV. Scale Bar:100μm. (B) Orthogonal slice projections of the edge (left) and center (right) of Thy1:YFP *ex vivo* tissue fixed at 14DEV. C) Orthogonal slice projections of the edge (left) and center (right) of Rlbp1:eGFP *ex vivo* tissue fixed at 1DEV. (D) Orthogonal slice projections of the edge (left) and center (right) of Rlbp1:eGFP *ex vivo* tissue fixed at 14DEV. (N=4).

Figure 5. BrdU incorporation increases with electrical stimulation in the *ex vivo* retina. (A) Timeline of experimental design for tissue electroporated at 1DEV and 14DEV. BrdU is delivered in culture medium for 24 hours. Following fixation, pieces of retinal tissue were cut, stained for BrdU incorporation, and imaged using confocal microscopy. No Electroporation (-*EP*) retinas were given BrdU and fixed at the same timepoints indicated for electroporated retinas (+*EP, +EP*^{DNA}). (B) BrdU incorporation -*EP* (left), +*EP* (center) and +*EP*^{DNA} (right) retinas at 1DEV (top) and 14DEV (bottom). Scale Bar: 100μm. (C) Quantification of the number of BrdU+ cells detected per tissue volume (mm^3). Mean ± SEM is shown. N=5-10. *$p < 0.05$, **$p < 0.01$, ***$p < 0.001$, ****$p < 0.0001$. No bracket indicates $p > 0.05$. All statistical tests performed on arcsine transformed values.

422 **Figure 6. Increase in BrdU+ Müller glia at 14DEV vs. 1DEV and following electrical**
423 **stimulus.** (A) 1DEV *-EP* (left) or *+EP* (right) retinas stained for IBA1 (top left) or SOX9
424 (bottom left) and BrdU (top middle & bottom middle). Overlap of IBA1 & BrdU (top right)
425 or SOX9 & BrdU (bottom right). Arrows indicate double labeled cells. Scale bar: 50µm.
426 (B) 14DEV *-EP* (left) or *+EP* (right) retinas stained for IBA1 (top left) or SOX9 (bottom
427 left) and BrdU (top middle & bottom middle). Overlap of IBA1 & BrdU (top right) or
428 SOX9 & BrdU (bottom right). Colabeled cells appear white. Scale bar: 50µm. (C)
429 Quantification of the percent of BrdU+ cells that are IBA1+ (left) or SOX9+ (right) in *-EP*
430 and *+EP* conditions at 1DEV and 14DEV. D) Quantification of colabeled IBA1+ (left) or
431 SOX9+ (right) cells colabeled as BrdU+ per tissue volume (mm^3) in *-EP* and *+EP*
432 conditions at 1DEV and 14DEV. Mean ± SEM is shown. N=5-10. *$p < 0.05$, **$p < 0.01$,
433 ***$p < 0.001$, ****$p < 0.0001$. No bracket indicates $p > 0.05$. All statistical tests
434 performed on arcsine transformed values.
435
436 **Figure 7. Co-transfection pCMV-eGFP and pCMV-Cre reveals increased**
437 **detectability of transfected cells with a Cre expression construct.** (A) Schematic of
438 detection of pCMV-eGFP expression (left) vs. pCMV-Cre expression (right) in a *Rosa*^{AI14}
439 reporter tissue when few or many copies of the construct are transfected in a cell. (B)
440 Cells transfected with equimolar concentration of pCMV-CRE and pCMV-eGFP at
441 1DEV at the center (left) or edge (right). Scale bar: 100µm. (C) Cells transfected with
442 equimolar concentration of pCMV-CRE and pCMV-eGFP at 14DEV at the center (left)
443 or edge (right) of retinas electroporated at 14DEV with both constructs at equimolar
444 concentration. Scale bar: 100µm. (D) Quantification of the proportion (%) of colabeled

445 cells detectable as transfected with pCMV-eGFP (eGFP+) and pCMV-Cre (tdTom+)
446 within eGFP+ or tdTom+ populations transfected at 1DEV (left) and 14DEV (right).. (E)
447 Quantification of the proportion (%) of cells detectable as transfected with pCMV-eGFP
448 (eGFP+) and pCMV-Cre (tdTom+) within the population of all cells transfected at 1DEV
449 (left) and 14DEV (right). Mean ± SEM is shown. N=4. *$p < 0.05$, **$p < 0.01$, ***$p < 0.001$,
450 ****$p < 0.0001$. No bracket indicates $p > 0.05$. All statistical tests performed on arcsine
451 transformed values.

452 **Figure 8. Variation in transfection efficiency in constructs with different**
453 **expression elements.** (A) Cells transfected with equimolar concentration of pCAG-Cre
454 and pCMV-eGFP at 1DEV (top) and 14DEV (bottom) Scale bar: 100μm. (B)
455 Quantification of the proportion (%) of colabeled cells detectable as co-transfected with
456 pCMV-eGFP (eGFP+) and pCAG-Cre (tdTom+) within total eGFP+ or tdTom+
457 populations at 1DEV (left) and 14DEV (right). C) Quantification of the proportion (%) of
458 cells detectable as transfected with pCMV-eGFP (eGFP+) and pCAG-Cre (tdTom+)
459 within the population of all transfected cells at 1DEV (left) and 14DEV (right). (D) Cells
460 transfected with equimolar concentration of pEF1α-Cre and pCMV-eGFP at 1DEV (top)
461 and 14DEV (bottom) Scale bar: 100μm. (E) Quantification of the proportion (%) of
462 colabeled cells detectable as co-transfected with pCMV-eGFP (eGFP+) and pEF1α-Cre
463 (tdTom+) within total eGFP+ or tdTom+ populations at 1DEV (left) and 14DEV (right).
464 (F) Quantification of the proportion (%) of cells detectable as transfected with pCMV-
465 eGFP (eGFP+) and pEF1α-Cre (tdTom+) within the population of all transfected cells at
466 1DEV (left) and 14DEV (right). (G) Quantification of ratio of tdTom+ cells to eGFP+ cells
467 at 1DEV and 14DEV in retinas co-transfected with pCMV-eGFP and either pCMV-Cre,

468 pCAG-Cre or pEF1α-Cre. Mean ± SEM is shown. N=3-4. *$p < 0.05$, **$p < 0.01$, ***$p <$
469 0.001, ****$p < 0.0001$. No bracket indicates $p > 0.05$. Statistical tests performed on
470 arcsine transformed values in B, C, E and F. The Y-Axis is Log_2 transformed in G.

471

472 **STAR Methods**

473 **I. Resource Availability**

474 **Lead Contact**

475 Further information and requests for resources and reagents should be directed
476 to EML.

477

478 **Materials Availability**

479 This study did not generate new unique reagents.

480

481 **Data and code availability**

482 Microscopy and quantification data reported in this paper will be shared upon
483 request.

484

485 **II. Experimental model and participant details**

486 **Mice**

487 B6/129 mice (Jackson Laboratory (#101043)): 8 weeks old, female.

488

489 Thy-1 YFP-16 (B6.Cg-Tg(Thy1-YFP)16Jrs/J) (Jackson Laboratory (#003709)): 8 to 12
490 weeks old, female and male.

Rlbp1-eGFP (Tg(Rlbp1-eGFP)1Eml (MGI: 6195229)): 8 to 12 weeks old, female and male.

Rlbp1-CreERT2; Rosa^{Ai14} (129S6.Cg-Tg(Rlbp1-cre/ERT2)1Tfur (MGI:Pending); B6.Cg-*Gt(ROSA)26Sor*$^{tm14(CAG\text{-}tdTomato)Hze}$/J (Jackson Laboratory (#007914))), 8 to 12 weeks old, female and male.

All mice are co-housed in a 12h/12h light-dark cycle with water and food ad libitum. All transgenic mice are backcrossed to B/129 mice. All animal experiments with mice were approved under the protocol M1600235 by the Vanderbilt Institutional Animal Care and Use committee and conform to the ARVO guidelines for the use of animals in vision research. All possible efforts were made to minimize animal suffering and the number of animals used.

III. Method Details

Tamoxifen administration

To activate Cre recombination in transgenic mice, 2 doses of 200μg per gram body weight (GBW) of tamoxifen (Sigma Aldrich, T2859) were delivered in corn oil (Sigma Aldrich, C8267) via oral gavage. Mice were euthanized for tissue collection at least 5 days after tamoxifen treatment.

Retinal dissection

513 Prior to tissue harvest, dissection tools were sterilized with 70% ethanol and UV
514 light for 15 minutes, and workstation was sterilized with 70% ethanol. 1X HBSS with
515 Ca^{2+} and Mg^{2+} (Gibco, 14025) with 10mM HEPEs (Sigma Aldrich, H0887) and 1X
516 Antibiotics-Antimycotics (Gibco, 15240062) (referred to as HBSS hereon) was prepared
517 and kept on ice. Mice were euthanized by CO_2 asphyxiation and cervical dislocation.
518 Each eye was enucleated, rinsed in cold HBSS, then transferred to a fresh HBSS dish.
519 Under a dissection scope and on a cold plate to keep retinas chilled, an incision was
520 made in the cornea. The cornea was removed using spring scissors. The sclera,
521 choroid and RPE were removed, the optic nerve head was cut on the proximal side with
522 spring scissors, leaving it intact in the retina, and the retina and lens were transferred to
523 a fresh HBSS dish. The lens was removed. Using spring scissors, 4 incisions were cut
524 into retinal tissue from periphery through 25-40% of tissue toward optic nerve head,
525 creating a flower-shaped retinal tissue that can be flattened.
526
527 ***Ex vivo* retinal explant tissue culture**
528 On the day of culture, plating media with supplements was prepared:
529 NeuroCult™ Plating Media (Stem Cell Technologies, 05713), 1X SM1 neuronal
530 supplement (Stem Cell Technologies, 05711) , 500μM L-Glutamine (Gibco, 25030149),
531 and 100unit Penicillin/100μg Streptomycin (Pen/Strep) (ThermoFisher, 15140) (referred
532 to as plating media hereon).
533 Retinal tissue was dissected as described above. A hydrophilic PTFE cell culture
534 insert (Millicell, PICM0RG50) was prepared by pipetting 150uL of plating media onto
535 insert membrane. Retinal tissue was mounted onto the PTFE membrane with the retinal

536 apical surface (photoreceptor side) in juxtaposition. Tissue was placed into a 6-well
537 plate (Corning, 353004) containing 1mL plating media and incubated at 37°C with 5%
538 CO^2. After 48 hours, 500uL of initial plating media was replaced with BrainPhys™
539 Neuronal Medium (Stem Cell Technologies, 05790) containing 1X SM1 neuronal
540 supplement, 1X N2 Supplement-A (Stem Cell Technologies, 07152) and Pen/Strep
541 (referred to as BrainPhys media hereon). 500µL of media was removed and replaced
542 with fresh BrainPhys media every 48 hours for the extent of the culture.
543
544 **Agarose Disk Electroporation**
545 0.5% agarose (RPI, A20090) in 1X PBS was heated to dissolve. 500µL was
546 pipetted into multiple wells of a 24-well plate (Corning, CLS3516) and left to solidify at
547 room temperature for 30 minutes in a cell culture hood. An anode dish was made by
548 lining a 100mm dish (Sigma Aldrich, Z358762) with aluminum foil, sterilized under UV
549 light for 15 minutes, and connected to the electroporator (BTX, 45-0052) by clamping
550 the anode cable onto the aluminum foil. Sterile, chilled PBS was pipetted onto the
551 anode dish. Tools and workspace were sterilized with 70% ethanol. The PTFE insert
552 containing the tissue culture was washed by gently dipping the membrane in fresh,
553 sterile PBS. The PTFE insert was then placed on the PBS in the anode dish.
554 An arm electrode (Bulldog Bio, CUY700P7L) connected to the electroporator was
555 mounted on a micromanipulator (Narishige, UMM-3C) with the electrode surface facing
556 up. Using a plastic transfer pipet (Fisherbrand, 13-711-7M) cut above the tapered tip, an
557 agarose disk was stamped from the solidified agarose and transferred using a spatula

558 to the arm electrode face. The disk was gently pressed to ensure adherence without
559 bubbles underneath.

560 The 12μL DNA-glycerol transfection solution was prepared using a combination
561 of 3pMol plasmid DNA diluted in sterile PBS with 7.5% glycerol (Sigma Aldrich, C8267),
562 and 2.5% methyl green dye (MCE, HYD0163). The DNA-Glycerol solution was pipetted
563 on top of the agarose disk and the arm electrode was rotated 180° while the DNA-
564 glycerol solution and the agarose disk stayed adhered via surface tension. The arm
565 electrode was lowered until the DNA solution was in contact with the tissue. Once there
566 is contact between all components of the system, a closed circuit is formed.

567 Each tissue was electroporated with five square wave pulses (25V) for 50ms
568 each with 250ms intervals between pulses. The arm electrode was slowly raised to
569 disconnect from the tissue, and the tissue was returned to the incubator. This protocol
570 has only been tested with square wave pulses.

571 Expression construct pCMV-eGFP was generated by the Levine lab. pCMV-
572 mCherry was a gift from Roger Tsien (ClonTech plasmid # 632524,
573 https://www.takarabio.com/documents/Vector%20Documents/PT3975-5_060412.pdf).
574 pCMV-Cre was a gift from David Liu (Addgene plasmid # 123133 ;
575 http://n2t.net/addgene:123133 ; RRID:Addgene_123133). pCAG-Cre was a gift from
576 Anjen Chenn (Addgene plasmid # 26647 ; http://n2t.net/addgene:26647 ;
577 RRID:Addgene_26647), which was generated by Anjen Chenn by insertion of the Cre
578 expression motif and deletion of the GFP expression motif into the backbone of pCAG-
579 GFP, a gift from Connie Cepko (Addgene plasmid # 11150 ;
580 http://n2t.net/addgene:11150 ; RRID:Addgene_11150). pBS513 EF1alpha-cre was a gift

581 from Brian Sauer (Addgene plasmid # 11918 ; http://n2t.net/addgene:11918 ;
582 RRID:Addgene_11918).
583
584 **Retinal explant culture tissue fixation**
585 Culture medium was removed and replaced with room temperature PBS to wash
586 3 times for 10 minutes each. 100μL 1X PBS was pipetted on top of tissue for each
587 wash. Retinas were fixed in 4% PFA for 2 hours at room temperature or at 4°C for 24
588 hours. PFA was removed and fixed retinas were washed 3 times with 1 mL 1X PBS for
589 30 minutes at room temperature. Fixed retinas were stored at 4°C in 1 mL 1X PBS with
590 0.01% sodium azide (Sigma Aldrich, 08591).
591
592 **Whole mount immunohistochemistry**
593 Each quadrant of the retinal tissue was separated and cut in half to generate 8
594 tissue fragments for staining. Individual tissue fragments were transferred into a 96-well
595 plate (Corning, CLS3628). Retinas were washed 3 times with 1mL 1X PBS containing
596 1% Triton-X (1% PBST), followed by 100μL 10% normal donkey serum (NDS)
597 (SouthernBiotech, 003001) in 1% PBST (blocking buffer) for 2 hours at room
598 temperature. Blocking buffer was removed and retinas were stained with primary
599 antibodies in 1% NDS blocking buffer for 2 hours at room temperature or 24 hours at
600 4°C. Retinas were washed 3 times with 200μL 1% PBST for 30 minutes each.
601 Secondary antibodies in 1% NDS blocking buffer were applied for 2 hours at room
602 temperature. The secondary antibody was removed, and tissue was washed 3 times
603 with 200μL 1% PBST for 30 minutes per wash. Stained retinas were mounted on

604 Colorfrost plus slides (Fisherbrand, 12-550-17) in Fluoromount G (Invitrogen, 00-4958-
605 02), coversliped, allowed to dry at room temperature overnight, then stored at 4°C until
606 imaged.
607 The following primary antibodies were used: α-BrdU (1:200, Abcam, ab6326), α-
608 IBA1 (1:500, FUJIFILM, 019-19741), and α-SOX9 (1:500, Chemicon, ab5535).
609 Secondary antibodies conjugated to Alexa 488 (Invitrogen, A21206), Alexa 568
610 (Invitrogen, A10042), and Alexa 647 (Intvitrogen, 21247) were each diluted at 1:500.
611
612 **BrdU treatment and detection**
613 16μM BrdU was added to culture media at varying timepoints in culture per
614 experiment. BrdU media was replenished daily until fixation. *Ex vivo* retinas were
615 treated with BrdU for 24-72 hours depending on the experiment. Following treatment,
616 tissues were fixed with PFA as described above. A 1/8 piece of tissue was selected at
617 random and cut using as scalpel from the retinal culture to stain. Retinas were
618 immunostained as described above for all other immunomarkers, then fixed with PFA
619 for 30 min to preserve antigens prior to BrdU immunostaining. 2N HCl (Fisher Scientific,
620 SA541) was used for antigen retrieval for 45 minutes at room temperature, followed by
621 a 20-minute neutralization with 0.1M sodium borate (pH 8.5) (Millipore Sigma,
622 1066690010).
623
624 **Imaging**
625 Cultures were imaged using a fluorescent stereoscope (Nikon SMZ1270i) every
626 48 hours post-culture establishment, and every 24 hours post-electroporation monitor

627 for morphological, structural, or fluorescent protein expression changes within the
628 tissue. The Zeiss LSM 710 confocal microscope was used to image tissue cultures after
629 fixation alone or fixation and staining. Images were analyzed using FIJI version 2.9.0.
630

631 **Orthogonal slice projections**

632 To observe structural changes in *ex vivo* retinal tissue cultures, 40X Z-Stack
633 images were obtained from the Zeiss LSM 710 confocal microscope with 1μm steps
634 between Z slices. Using FIJI version 2.9.0, 354.25 by 11.76 pixel ROIs were selected at
635 random but angled from tissue periphery toward optic nerve head. These ROIs were
636 converted to 3D projections and rotated to view as a cross section.
637

638 **IV. Quantification and Statistical Analysis**

639 All cell counting and tissue volume calculations were calculated from 20X Z-
640 stack, tile confocal images using Imaris 10.1 software. No statistical methods were used
641 to predetermine sample sizes. GraphPad Prism 10 was used for the following statistical
642 tests: All proportion values were arcsine transformed prior to statistical analysis.
643 Comparisons between more than two groups were made by two-way ANOVA with
644 Tukey post-hoc test. Comparisons between two groups within the same tissue, as in
645 figure 7, were made using paired two-tailed t tests. Differences were considered
646 statistically significant at $p < 0.05$. Data are presented as mean ± SEM. Statistical
647 significance is indicated with asterisks: *$p < 0.05$, **$p < 0.01$, ***$p < 0.001$, ****$p <$
648 0.0001. Figure graphics created using Biorender.
649

650 **Supplemental Information**

651 **Document S1. Figure S1 and Table S1**

652 **Figure S1: Proportion of eGFP+ and tdTom+ cells in tissues transfected with**
653 **pCMV-eGFP and Cre expression construct with differing elements.** Euler plots of
654 the proportion (%) of eGFP+, tdTom+, and eGFP+ tdTom+ colabeled cells per the sum
655 of an edge and center $6.02x10^7$ um^3 ROI. Retinas transfected at 1DEV (top) and 14DEV
656 (bottom) with pCMV-eGFP and pCMV-Cre (left), pCAG-Cre (middle) or pEF1α-Cre
657 (right). Euler plots are scaled to represent proportion. N=3-4. Statistical information
658 available in Table S1.

659

660 **Table S1: Quantification of cells transfected at 1DEV and 14DEV with pCMV-eGFP**
661 **and pCMV-Cre, pCAG-Cre or pEF1α-Cre.** Cell counts calculated from sum of cells
662 detected in a 6.02x107 um3 region of interest at center and edge of each retinal
663 sample. ROIs were selected based on presence of transfected cells. The negative
664 inverse is shown for tdTom:eGFP ratios in which there were more eGFP+ cells than
665 tdTom+ cells.

666

667 **References**

668 1. Lucas RJ. Mammalian Inner Retinal Photoreception. *Curr Biol*. 2013;23(3):R125-R133.
669 doi:10.1016/j.cub.2012.12.029

670 2. Vecino E, Rodriguez FD, Ruzafa N, Pereiro X, Sharma SC. Glia–neuron interactions in the
671 mammalian retina. *Prog Retin Eye Res*. 2016;51:1-40. doi:10.1016/j.preteyeres.2015.06.003

672 3. Hu Y, Wang X, Hu B, et al. Dissecting the transcriptome landscape of the human fetal neural
673 retina and retinal pigment epithelium by single-cell RNA-seq analysis. *PLoS Biol*.
674 2019;17(7):e3000365. doi:10.1371/journal.pbio.3000365

675 4. Cornwall MC, Fein A, Macnichol Jr. EM. Cellular mechanisms that underlie bleaching and
676 background adaptation. *J Gen Physiol*. 1990;96(2):345-372.

677 5. Sparrow JR, Parish CA, Hashimoto M, Nakanishi K. A2E, a Lipofuscin Fluorophore, in Human
678 Retinal Pigmented Epithelial Cells in Culture. *Invest Ophthalmol Vis Sci*. 1999;40(12):2988-
679 2995.

680 6. Ueki Y, Karl MO, Sudar S, et al. P53 is required for the developmental restriction in Müller
681 glial proliferation in mouse retina. *Glia*. 2012;60(10):1579-1589. doi:10.1002/glia.22377

682 7. Lee JE, Liang KJ, Fariss RN, Wong WT. Ex vivo Dynamic Imaging of Retinal Microglia using
683 Time-lapse Confocal Microscopy. *Invest Ophthalmol Vis Sci*. 2008;49(9):4169-4176.
684 doi:10.1167/iovs.08-2076

685 8. Jones MK, Lu B, Chen DZ, et al. In Vitro and In Vivo Proteomic Comparison of Human Neural
686 Progenitor Cell-Induced Photoreceptor Survival. *PROTEOMICS*. 2019;19(3):1800213.
687 doi:10.1002/pmic.201800213

688 9. Ueki Y, Reh TA. EGF stimulates müller glial proliferation via a BMP-dependent mechanism.
689 *Glia*. 2013;61(5):778-789. doi:10.1002/glia.22472

690 10. Löffler K, Schäfer P, Völkner M, Holdt T, Karl MO. Age-dependent Müller glia neurogenic
691 competence in the mouse retina. *Glia*. 2015;63(10):1809-1824. doi:10.1002/glia.22846

692 11. Schnichels S, Kiebler T, Hurst J, et al. Retinal Organ Cultures as Alternative Research Models.
693 *Altern Lab Anim*. 2019;47(1):19-29. doi:10.1177/0261192919840092

694 12. Schaeffer J, Delpech C, Albert F, Belin S, Nawabi H. Adult Mouse Retina Explants: From ex
695 vivo to in vivo Model of Central Nervous System Injuries. *Front Mol Neurosci*.
696 2020;13:599948. doi:10.3389/fnmol.2020.599948

697 13. Hong Yee C, Aoki S, Uchihashi K, et al. The Air Liquid-interface, a Skin Microenvironment,
698 Promotes Growth of Melanoma Cells, but not Their Apoptosis and Invasion, through
699 Activation of Mitogen-activated Protein Kinase. *Acta Histochem Cytochem*. 2010;43(1):1-7.
700 doi:10.1267/ahc.09036

701 14. Jiang D, Schaefer N, Chu HW. Air–Liquid Interface Culture of Human and Mouse Airway
702 Epithelial Cells. In: Alper S, Janssen WJ, eds. *Lung Innate Immunity and Inflammation:*
703 *Methods and Protocols*. Methods in Molecular Biology. Springer; 2018:91-109.
704 doi:10.1007/978-1-4939-8570-8_8

705 15. Pruniéras M, Régnier M, Woodley D. Methods for Cultivation of Keratinocytes with an Air-
706 Liquid Interface. *J Invest Dermatol*. 1983;81(1, Supplement):S28-S33. doi:10.1111/1523-
707 1747.ep12540324

708 16. Whitcutt MJ, Adler KB, Wu R. A biphasic chamber system for maintaining polarity of
709 differentiation of culture respiratory tract epithelial cells. *In Vitro Cell Dev Biol*.
710 1988;24(5):420-428. doi:10.1007/BF02628493

711 17. Verrill C, Davies J, Millward-Sadler H, Sundstrom L, Sheron N. Organotypic liver culture in a
712 fluid-air interface using slices of neonatal rat and adult human tissue—a model of fibrosis in
713 vitro. *J Pharmacol Toxicol Methods*. 2002;48(2):103-110. doi:10.1016/S1056-
714 8719(03)00042-X

715 18. Giandomenico SL, Mierau SB, Gibbons GM, et al. Cerebral organoids at the air–liquid
716 interface generate diverse nerve tracts with functional output. *Nat Neurosci*.
717 2019;22(4):669-679. doi:10.1038/s41593-019-0350-2

718 19. Cao X, Coyle JP, Xiong R, et al. Invited review: human air-liquid-interface organotypic airway
719 tissue models derived from primary tracheobronchial epithelial cells—overview and
720 perspectives. *Vitro Cell Dev Biol - Anim*. 2021;57(2):104-132. doi:10.1007/s11626-020-
721 00517-7

722 20. Venkatesh A, Ma S, Langellotto F, Gao G, Punzo C. Retinal gene delivery by rAAV and DNA
723 electroporation. *Curr Protoc Microbiol*. 2013;0 14:Unit-14D.4.
724 doi:10.1002/9780471729259.mc14d04s28

725 21. Ail D, Malki H, Zin EA, Dalkara D. Adeno-Associated Virus (AAV) - Based Gene Therapies for
726 Retinal Diseases: Where are We? *Appl Clin Genet*. 2023;16:111-130.
727 doi:10.2147/TACG.S383453

728 22. Matsuda T, Cepko CL. Electroporation and RNA interference in the rodent retina *in vivo* and
729 *in vitro*. *Proc Natl Acad Sci*. 2004;101(1):16-22. doi:10.1073/pnas.2235688100

730 23. Matsuda T, Cepko CL. Analysis of Gene Function in the Retina. In: Li S, ed. *Electroporation*
731 *Protocols*. Vol 423. Methods in Molecular Biology. Humana Press; 2008:259-278.
732 doi:10.1007/978-1-59745-194-9_19

733 24. Montana CL, Myers CA, Corbo JC. Quantifying the Activity of cis-Regulatory Elements in the
734 Mouse Retina by Explant Electroporation. *J Vis Exp*. 2011;(52):2821. doi:10.3791/2821

735 25. Jeon CJ, Strettoi E, Masland RH. The Major Cell Populations of the Mouse Retina. *J Neurosci*.
736 1998;18(21):8936-8946. doi:10.1523/JNEUROSCI.18-21-08936.1998

737 26. Mahabadi N, Khalili YA. Neuroanatomy, Retina. In: *StatPearls [Internet]*. StatPearls
738 Publishing; 2023. Accessed December 3, 2023.
739 https://www.ncbi.nlm.nih.gov/books/NBK545310/

740 27. Kato M, Sudou N, Nomura-Komoike K, Iida T, Fujieda H. Age- and cell cycle-related
741 expression patterns of transcription factors and cell cycle regulators in Müller glia. *Sci Rep*.
742 2022;12(1):19584. doi:10.1038/s41598-022-23855-w

743 28. Pellissier LP, Hoek RM, Vos RM, et al. Specific tools for targeting and expression in Müller
744 glial cells. *Mol Ther - Methods Clin Dev*. 2014;1. doi:10.1038/mtm.2014.9

745 29. Poché RA, Furuta Y, Chaboissier MC, Schedl A, Behringer RR. Sox9 Is Expressed in Mouse
746 Multipotent Retinal Progenitor Cells and Functions in Müller Glial Cell Development. *J Comp*
747 *Neurol*. 2008;510(3):237-250. doi:10.1002/cne.21746

748 30. Shaner NC, Campbell RE, Steinbach PA, Giepmans BNG, Palmer AE, Tsien RY. Improved
749 monomeric red, orange and yellow fluorescent proteins derived from Discosoma sp. red
750 fluorescent protein. *Nat Biotechnol*. 2004;22(12):1567-1572. doi:10.1038/nbt1037

751 31. Feng G, Mellor RH, Bernstein M, et al. Imaging neuronal subsets in transgenic mice
752 expressing multiple spectral variants of GFP. *Neuron*. 2000;28(1):41-51. doi:10.1016/s0896-
753 6273(00)00084-2

754 32. Vazquez-Chona FR, Clark AM, Levine EM. *Rlbp1* Promoter Drives Robust Müller Glial GFP
755 Expression in Transgenic Mice. *Investig Opthalmology Vis Sci*. 2009;50(8):3996.
756 doi:10.1167/iovs.08-3189

757 33. Wang J, O'Sullivan ML, Mukherjee D, Puñal VM, Farsiu S, Kay JN. Anatomy and spatial
758 organization of Müller glia in mouse retina. *J Comp Neurol*. 2017;525(8):1759-1777.
759 doi:10.1002/cne.24153

760 34. Rashid K, Akhtar-Schaefer I, Langmann T. Microglia in Retinal Degeneration. *Front Immunol*.
761 2019;10:1975. doi:10.3389/fimmu.2019.01975

762 35. Wohl SG, Schmeer CW, Witte OW, Isenmann S. Proliferative Response of Microglia and
763 Macrophages in the Adult Mouse Eye after Optic Nerve Lesion. *Investig Opthalmology Vis*
764 *Sci*. 2010;51(5):2686. doi:10.1167/iovs.09-4537

765 36. Vázquez-Chona FR, Swan A, Ferrell WD, et al. Proliferative reactive gliosis is compatible with
766 glial metabolic support and neuronal function. *BMC Neurosci*. 2011;12(1):98.
767 doi:10.1186/1471-2202-12-98

768 37. Nomura-Komoike K, Saitoh F, Komoike Y, Fujieda H. DNA Damage Response in Proliferating
769 Müller Glia in the Mammalian Retina. *Investig Opthalmology Vis Sci*. 2016;57(3):1169.
770 doi:10.1167/iovs.15-18101

771 38. Goldman D. Müller glia cell reprogramming and retina regeneration. *Nat Rev Neurosci*.
772 2014;15(7):431-442. doi:10.1038/nrn3723

773 39. Hoang T, Wang J, Boyd P, et al. Gene regulatory networks controlling vertebrate retinal
774 regeneration. *Science*. 2020;370(6519):eabb8598. doi:10.1126/science.abb8598

775 40. Chen C, Bai X, Ding Y, Lee IS. Electrical stimulation as a novel tool for regulating cell
776 behavior in tissue engineering. *Biomater Res*. 2019;23:25. doi:10.1186/s40824-019-0176-8

41. Hernández-Bule ML, Paíno CL, Trillo MÁ, Úbeda A. Electric Stimulation at 448 kHz Promotes Proliferation of Human Mesenchymal Stem Cells. *Cell Physiol Biochem*. 2014;34(5):1741-1755. doi:10.1159/000366375

42. Katoh K. Effects of Electrical Stimulation of the Cell: Wound Healing, Cell Proliferation, Apoptosis, and Signal Transduction. *Med Sci*. 2023;11(1):11. doi:10.3390/medsci11010011

43. Liu M, Xie D, Zeng H, Zhai N, Liu L, Yan H. Direct-current electric field stimulation promotes proliferation and maintains stemness of mesenchymal stem cells. *BioTechniques*. 2023;74(6):293-301. doi:10.2144/btn-2022-0112

44. Martín D, Bocio-Nuñez J, Scagliusi SF, et al. DC electrical stimulation enhances proliferation and differentiation on N2a and MC3T3 cell lines. *J Biol Eng*. 2022;16(1):27. doi:10.1186/s13036-022-00306-8

45. Jullien N. Regulation of Cre recombinase by ligand-induced complementation of inactive fragments. *Nucleic Acids Res*. 2003;31(21):131e-1131. doi:10.1093/nar/gng131

46. Tian X, Zhou B. Strategies for site-specific recombination with high efficiency and precise spatiotemporal resolution. *J Biol Chem*. 2021;296:100509. doi:10.1016/j.jbc.2021.100509

47. Stachowski K, Norris AS, Potter D, Wysocki VH, Foster MP. Mechanisms of Cre recombinase synaptic complex assembly and activation illuminated by Cryo-EM. *Nucleic Acids Res*. 2022;50(3):1753-1769. doi:10.1093/nar/gkac032

48. Bessen JL, Afeyan LK, Dančík V, et al. High-resolution specificity profiling and off-target prediction for site-specific DNA recombinases. *Nat Commun*. 2019;10(1):1937. doi:10.1038/s41467-019-09987-0

49. Rodova M, Jayini R, Singasani R, Chipps E, Islam MR. CMV promoter is repressed by p53 and activated by JNK pathway. *Plasmid*. 2013;69(3):223-230. doi:10.1016/j.plasmid.2013.01.004

50. Bäck S, Dossat A, Parkkinen I, et al. Neuronal Activation Stimulates Cytomegalovirus Promoter-Driven Transgene Expression. *Mol Ther - Methods Clin Dev*. 2019;14:180-188. doi:10.1016/j.omtm.2019.06.006

51. Le Y, Miller JL, Sauer B. GFPcreFusion Vectors with Enhanced Expression. *Anal Biochem*. 1999;270(2):334-336. doi:10.1006/abio.1999.4110

52. Stollmeier M, Kahlert S, Zuschratter W, et al. Air-liquid interface cultures trigger a metabolic shift in intestinal epithelial cells (IPEC-1). *Histochem Cell Biol*. 2023;159(5):389-400. doi:10.1007/s00418-023-02180-x

53. Gueven N, Glatthaar B, Manke HG, Haemmerle H. Co-cultivation of rat pneumocytes and bovine endothelial cells on a liquid-air interface. *Eur Respir J*. 1996;9(5):968-975. doi:10.1183/09031936.96.09050968

811 54. Vera MS, Simón MV, Prado Spalm FH, et al. Ceramide-1-phosphate promotes the migration
812 of retina Müller glial cells. *Exp Eye Res*. 2021;202:108359. doi:10.1016/j.exer.2020.108359

813 55. Goldman D. Müller glial cell reprogramming and retina regeneration. *Nat Rev Neurosci*.
814 2014;15(7):431-442. doi:10.1038/nrn3723

815 56. Tackenberg MA, Tucker BA, Swift JS, et al. Müller cell activation, proliferation and migration
816 following laser injury. *Mol Vis*. 2009;15:1886-1896.

817 57. Bringmann A, Iandiev I, Pannicke T, et al. Cellular signaling and factors involved in Müller
818 cell gliosis: Neuroprotective and detrimental effects. *Prog Retin Eye Res*. 2009;28(6):423-
819 451. doi:10.1016/j.preteyeres.2009.07.001

820 58. Nomura-Komoike K, Saitoh F, Fujieda H. Phosphatidylserine recognition and Rac1 activation
821 are required for Müller glia proliferation, gliosis and phagocytosis after retinal injury. *Sci*
822 *Rep*. 2020;10(1):1488. doi:10.1038/s41598-020-58424-6

823 59. Jones BW, Watt CB, Frederick JM, et al. Retinal remodeling triggered by photoreceptor
824 degenerations. *J Comp Neurol*. 2003;464(1):1-16. doi:10.1002/cne.10703

825 60. Dobelle WH, Mladejovsky MG. Phosphenes produced by electrical stimulation of human
826 occipital cortex, and their application to the development of a prosthesis for the blind. *J*
827 *Physiol*. 1974;243(2):553-576. doi:10.1113/jphysiol.1974.sp010766

828 61. Chow AY, Chow VY, Packo KH, Pollack JS, Peyman GA, Schuchard R. The Artificial Silicon
829 Retina Microchip for the Treatment of VisionLoss From Retinitis Pigmentosa. *Arch*
830 *Ophthalmol*. 2004;122(4):460-469. doi:10.1001/archopht.122.4.460

831 62. Sato T, Fujikado T, Lee TS, Tano Y. Direct Effect of Electrical Stimulation on Induction of
832 Brain-Derived Neurotrophic Factor from Cultured Retinal Müller Cells. *Investig*
833 *Opthalmology Vis Sci*. 2008;49(10):4641. doi:10.1167/iovs.08-2049

834 63. Enayati S, Chang K, Achour H, et al. Electrical Stimulation Induces Retinal Müller Cell
835 Proliferation and Their Progenitor Cell Potential. *Cells*. 2020;9(3):781.
836 doi:10.3390/cells9030781

837 64. Kumar A, Nune K, Misra R. Understanding the response of pulsed electric field on osteoblast
838 functions in three-dimensional mesh structures. *J Biomater Appl*. 2016;31(4):594-605.
839 doi:10.1177/0885328216658376

840 65. Zhu W, Ye T, Lee SJ, et al. Enhanced neural stem cell functions in conductive annealed
841 carbon nanofibrous scaffolds with electrical stimulation. *Nanomedicine Nanotechnol Biol*
842 *Med*. 2018;14(7):2485-2494. doi:10.1016/j.nano.2017.03.018

843 66. Snyder S, DeJulius C, Willits RK. Electrical Stimulation Increases Random Migration of
844 Human Dermal Fibroblasts. *Ann Biomed Eng*. 2017;45(9):2049-2060. doi:10.1007/s10439-
845 017-1849-x

846 67. Zhao H, Steiger A, Nohner M, Ye H. Specific Intensity Direct Current (DC) Electric Field
847 Improves Neural Stem Cell Migration and Enhances Differentiation towards βIII-Tubulin+
848 Neurons. *PLoS ONE*. 2015;10(6):e0129625. doi:10.1371/journal.pone.0129625

849 68. Dong Z yong, Pei Z, Li Z, Wang Y ling, Khan A, Meng X ting. Electric field stimulation induced
850 neuronal differentiation of filum terminale derived neural progenitor cells. *Neurosci Lett*.
851 2017;651:109-115. doi:10.1016/j.neulet.2017.05.001

852 69. Ryan CNM, Doulgkeroglou MN, Zeugolis DI. Electric field stimulation for tissue engineering
853 applications. *BMC Biomed Eng*. 2021;3:1. doi:10.1186/s42490-020-00046-0

854

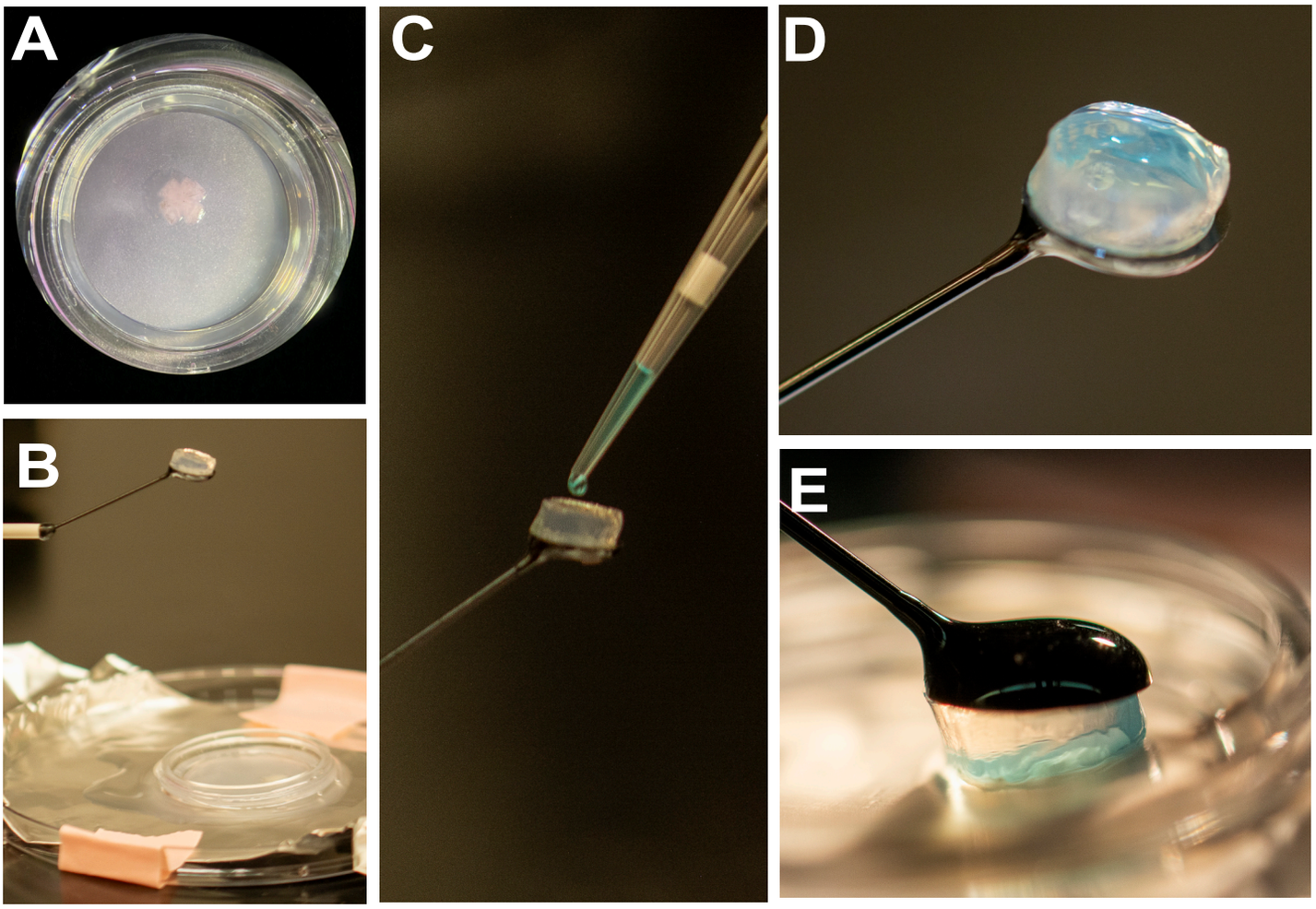
A
B
C
D
E

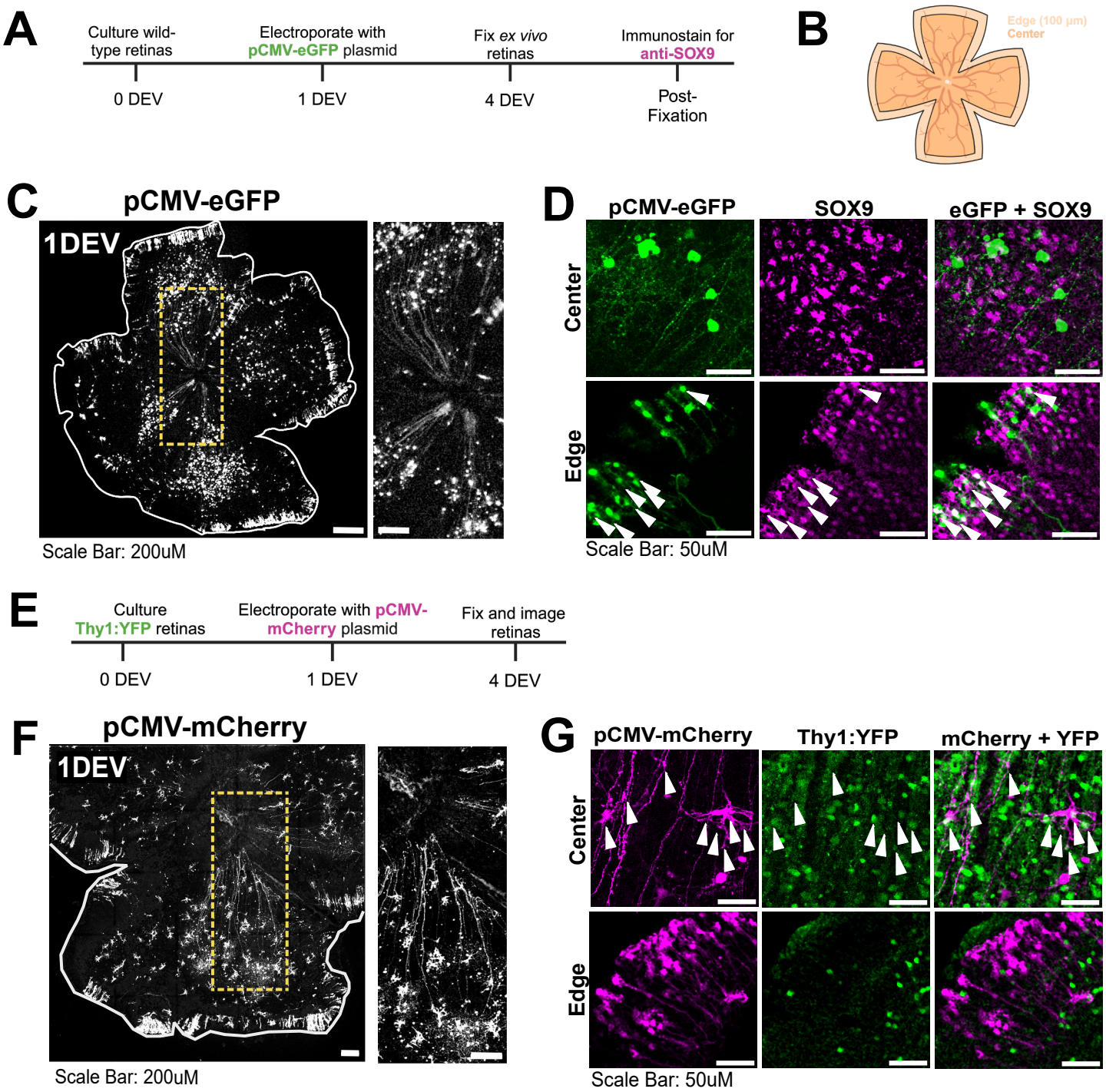
A
Culture wild-type retinas
Electroporate with pCMV-eGFP plasmid
Fix ex vivo retinas
Immunostain for anti-SOX9
0 DEV
1 DEV
4 DEV
Post-Fixation
B
Edge (100 µm)
Center
C
pCMV-eGFP
1DEV
Scale Bar: 200uM
D
pCMV-eGFP
SOX9
eGFP + SOX9
Center
Edge
Scale Bar: 50uM
E
Culture Thy1:YFP retinas
Electroporate with pCMV-mCherry plasmid
Fix and image retinas
0 DEV
1 DEV
4 DEV
F
pCMV-mCherry
1DEV
Scale Bar: 200uM
G
pCMV-mCherry
Thy1:YFP
mCherry + YFP
Center
Edge
Scale Bar: 50uM
H
1DEV
% transfected cells
100
80
60
40
20
0
**
****
****
**
****
***
Edge
Center
Edge & Center
transfected Müller glia
transfected neurons

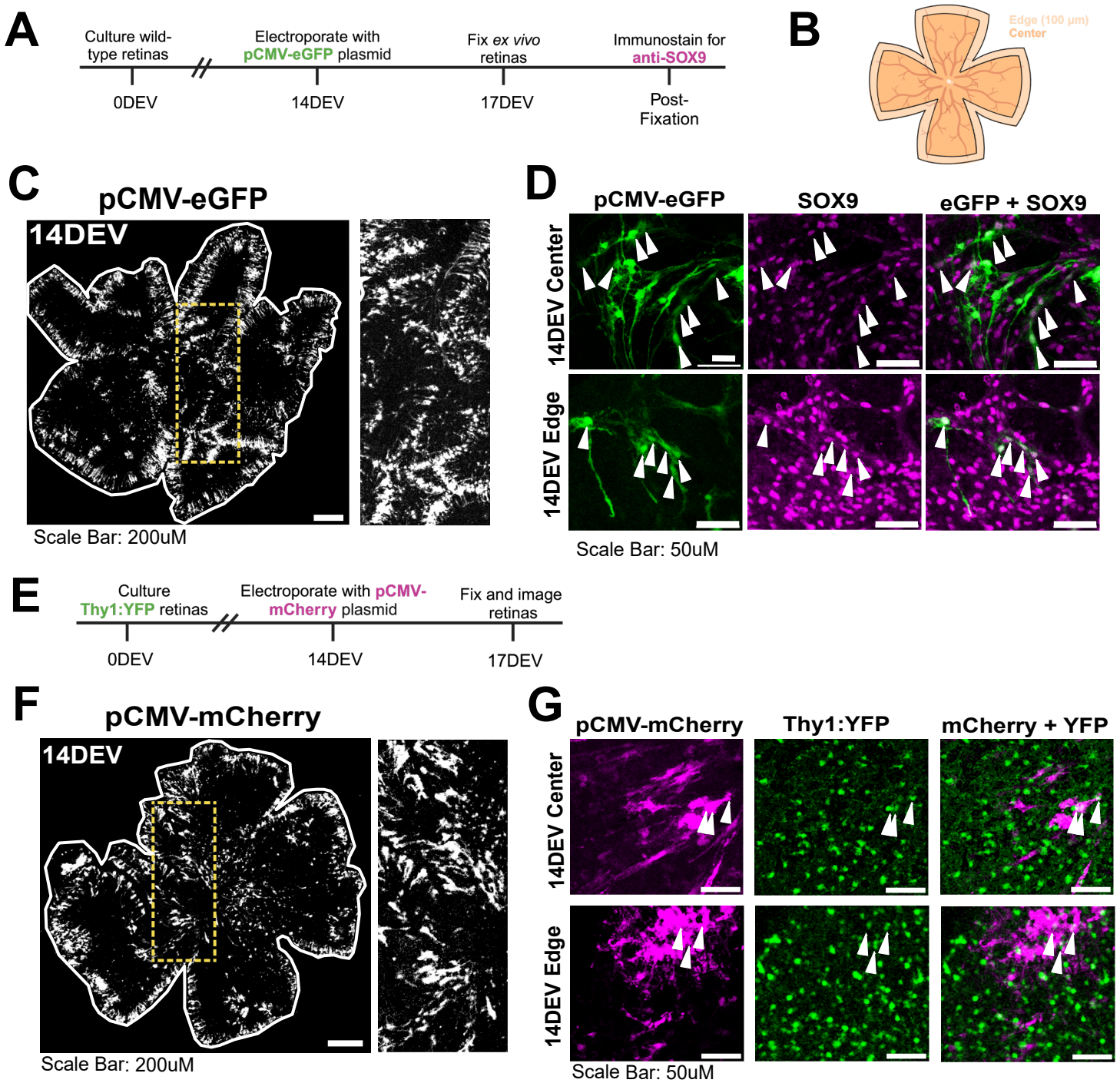
A
Culture wild-type retinas
Electroporate with pCMV-eGFP plasmid
Fix ex vivo retinas
Immunostain for anti-SOX9
0DEV
14DEV
17DEV
Post-Fixation
B
Edge (100 µm)
Center
C
pCMV-eGFP
14DEV
Scale Bar: 200uM
D
pCMV-eGFP
SOX9
eGFP + SOX9
14DEV Center
14DEV Edge
Scale Bar: 50uM
E
Culture Thy1:YFP retinas
Electroporate with pCMV-mCherry plasmid
Fix and image retinas
0DEV
14DEV
17DEV
F
pCMV-mCherry
14DEV
Scale Bar: 200uM
G
pCMV-mCherry
Thy1:YFP
mCherry + YFP
14DEV Center
14DEV Edge
Scale Bar: 50uM
H
14DEV
% transfected cells
100
80
60
40
20
0
****
****
****
Edge
Center
Edge & Center
transfected Müller glia
transfected neurons

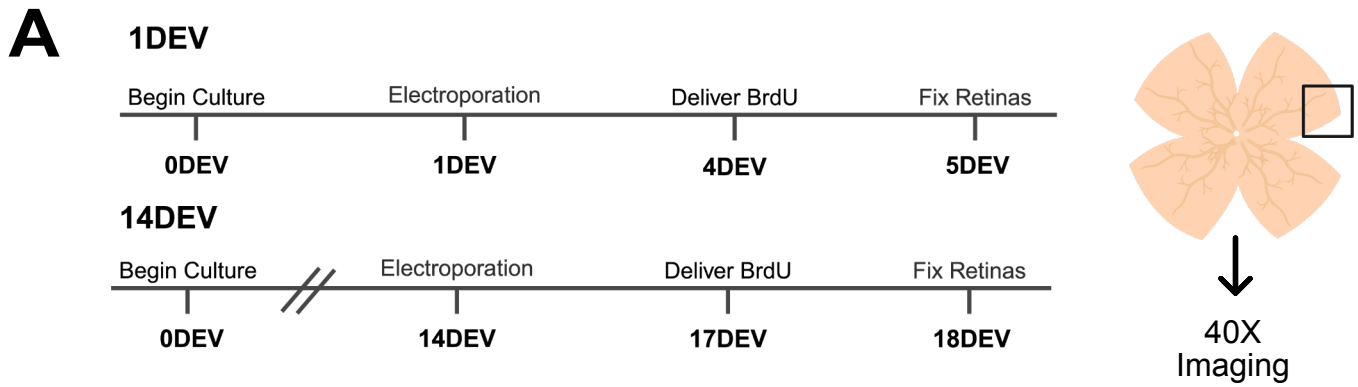
A
1DEV
Begin Culture
Electroporation
Deliver BrdU
Fix Retinas
0DEV
1DEV
4DEV
5DEV
14DEV
Begin Culture
Electroporation
Deliver BrdU
Fix Retinas
0DEV
14DEV
17DEV
18DEV
40X
Imaging

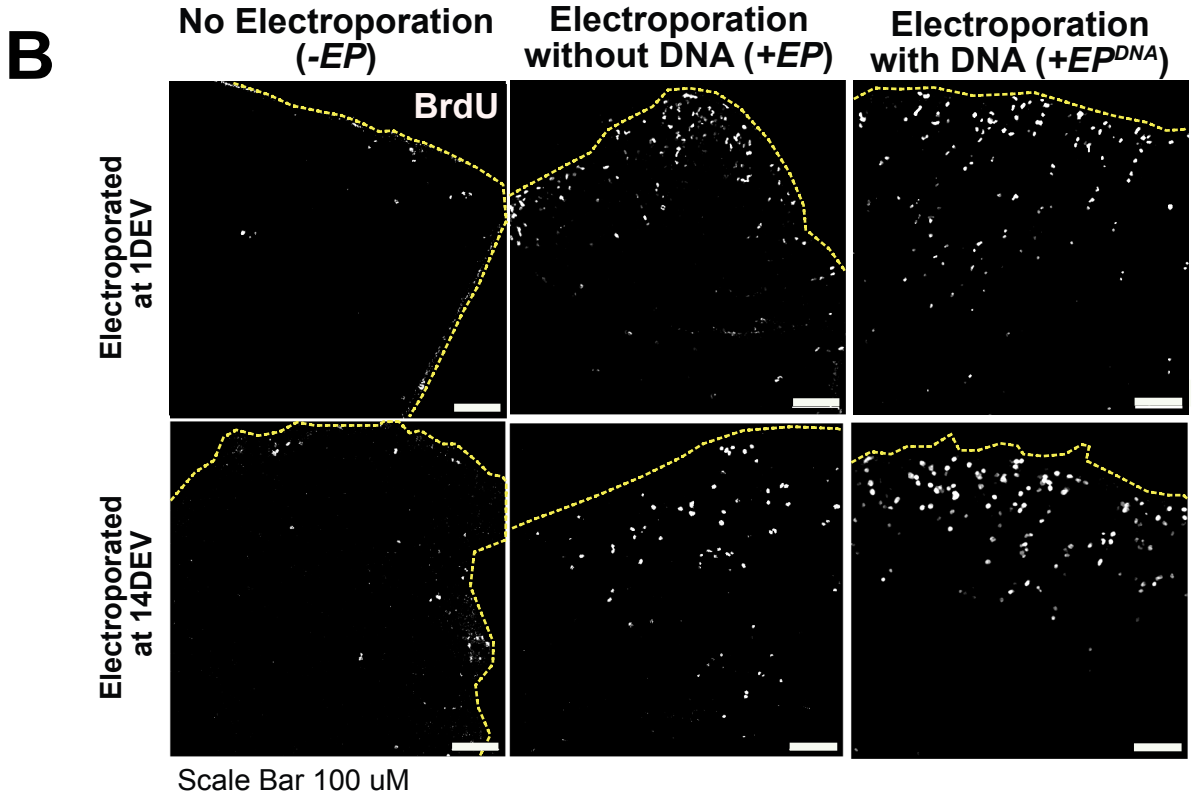
B
No Electroporation
(-EP)
Electroporation
without DNA (+EP)
Electroporation
with DNA (+EP^DNA)
BrdU
Electroporated
at 1DEV
Electroporated
at 14DEV
Scale Bar 100 uM

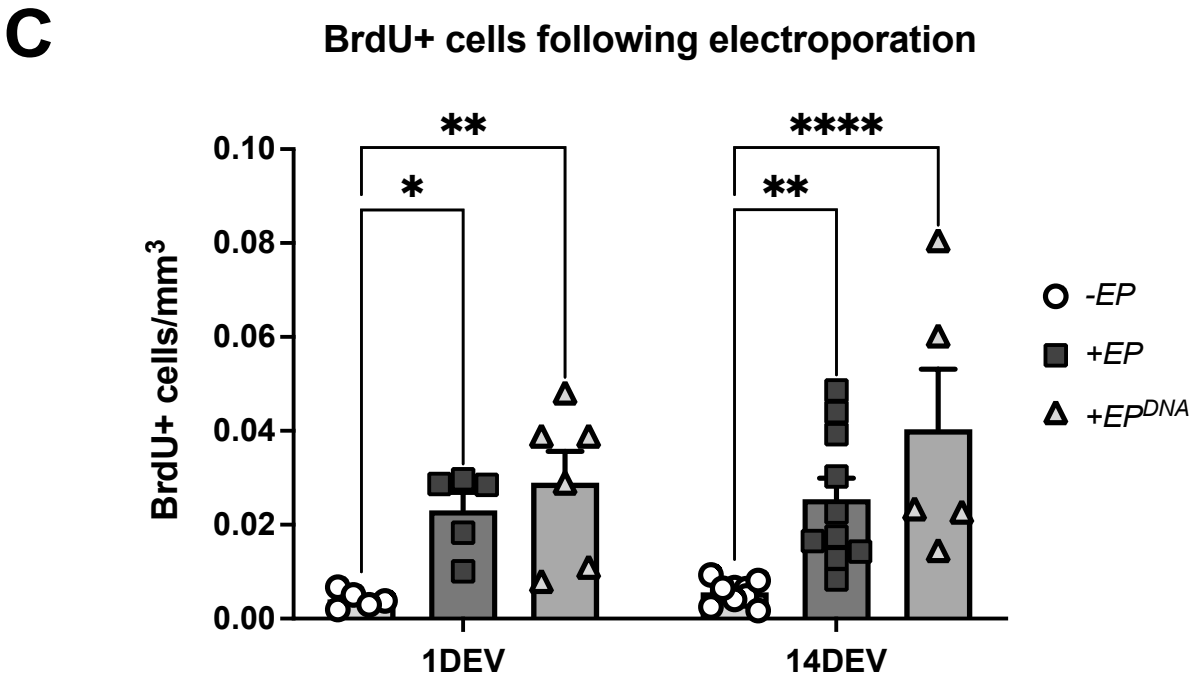
C
BrdU+ cells following electroporation
BrdU+ cells/mm3
0.10
0.08
0.06
0.04
0.02
0.00
**
*
****
**
1DEV
14DEV
-EP
+EP
+EP^DNA

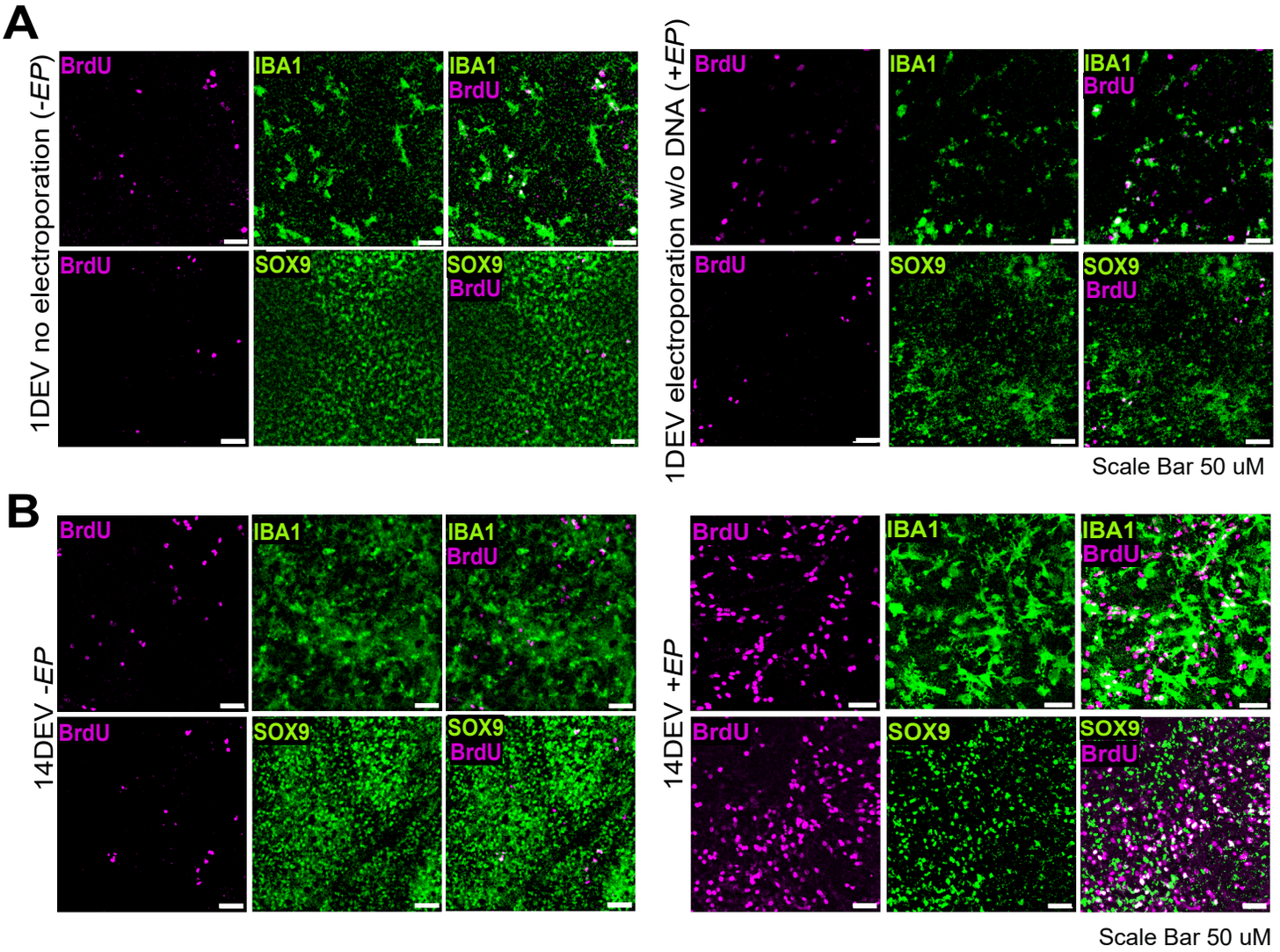
A
1DEV no electroporation (-EP)
1DEV electroporation w/o DNA (+EP)
BrdU
IBA1
IBA1 BrdU
SOX9
SOX9 BrdU
Scale Bar 50 uM
B
14DEV -EP
14DEV +EP
BrdU
IBA1
IBA1 BrdU
SOX9
SOX9 BrdU
Scale Bar 50 uM

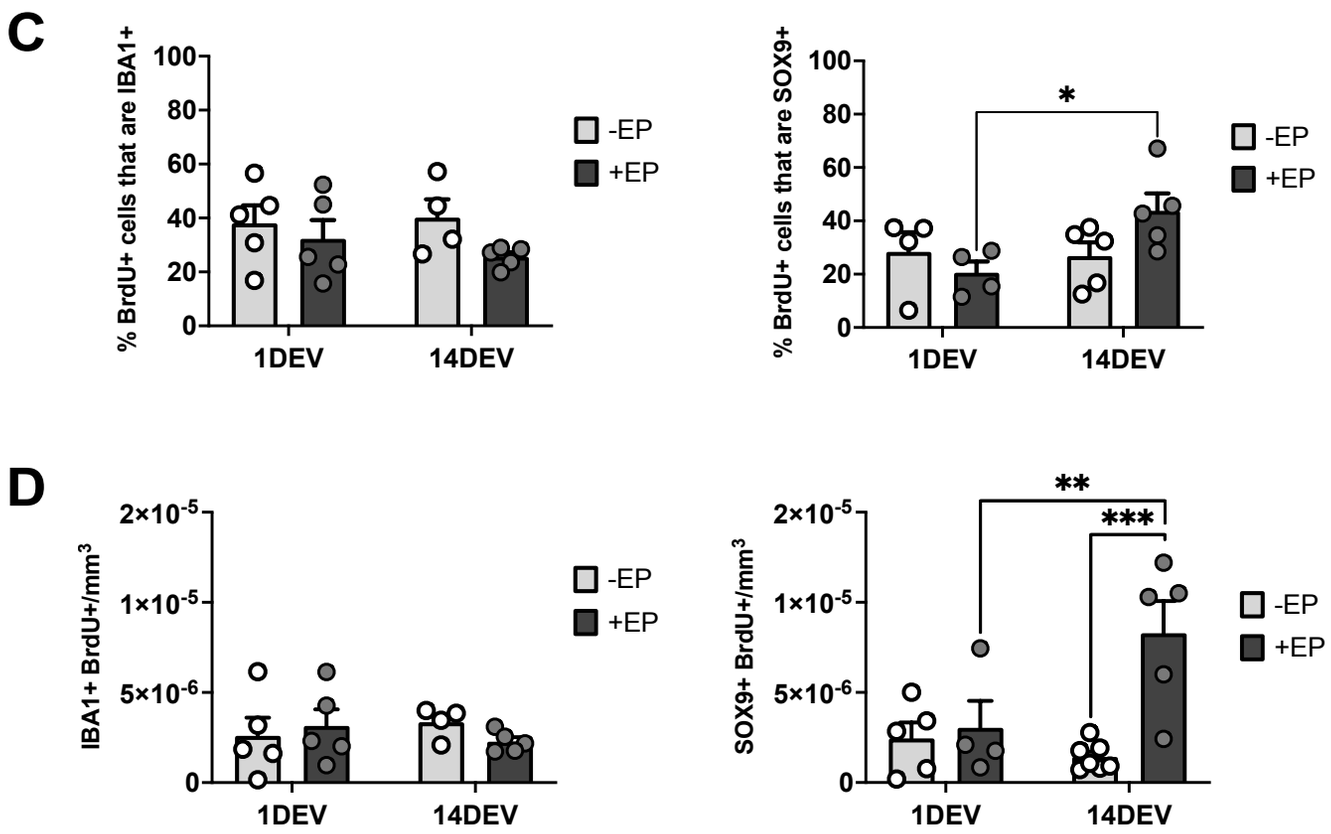
C
% BrdU+ cells that are IBA1+
% BrdU+ cells that are SOX9+
100
80
60
40
20
0
1DEV
14DEV
-EP
+EP
*
D
IBA1+ BrdU+/mm3
SOX9+ BrdU+/mm3
2×10-5
1×10-5
5×10-6
0
**
***

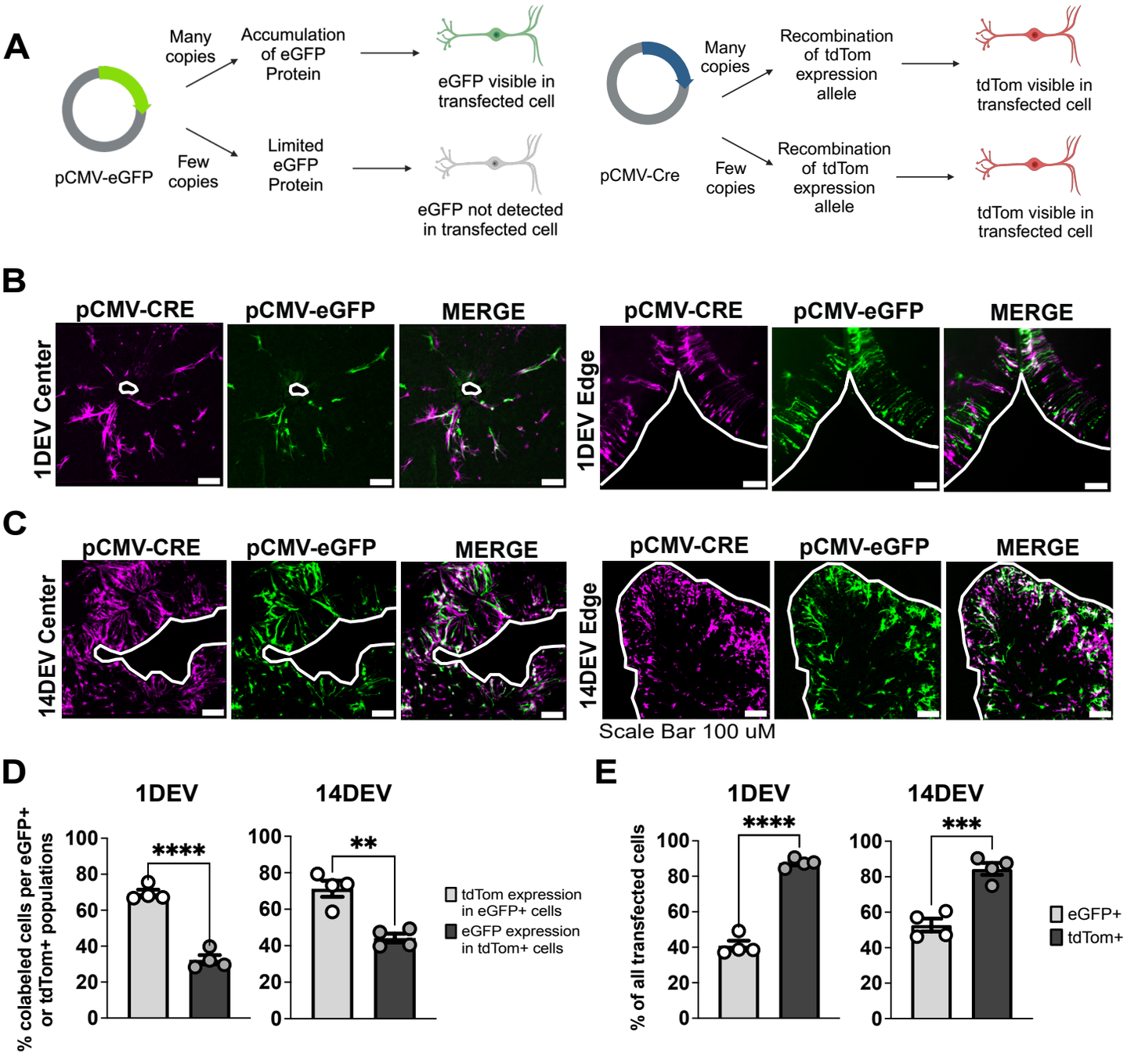
A
pCMV-eGFP
Many copies
Accumulation of eGFP Protein
eGFP visible in transfected cell
Few copies
Limited eGFP Protein
eGFP not detected in transfected cell
pCMV-Cre
Many copies
Recombination of tdTom expression allele
tdTom visible in transfected cell
Few copies
Recombination of tdTom expression allele
tdTom visible in transfected cell
B
pCMV-CRE
pCMV-eGFP
MERGE
1DEV Center
1DEV Edge
C
14DEV Center
14DEV Edge
Scale Bar 100 uM
D
1DEV
14DEV
% colabeled cells per eGFP+ or tdTom+ populations
****
**
tdTom expression in eGFP+ cells
eGFP expression in tdTom+ cells
E
% of all transfected cells
****
***
eGFP+
tdTom+

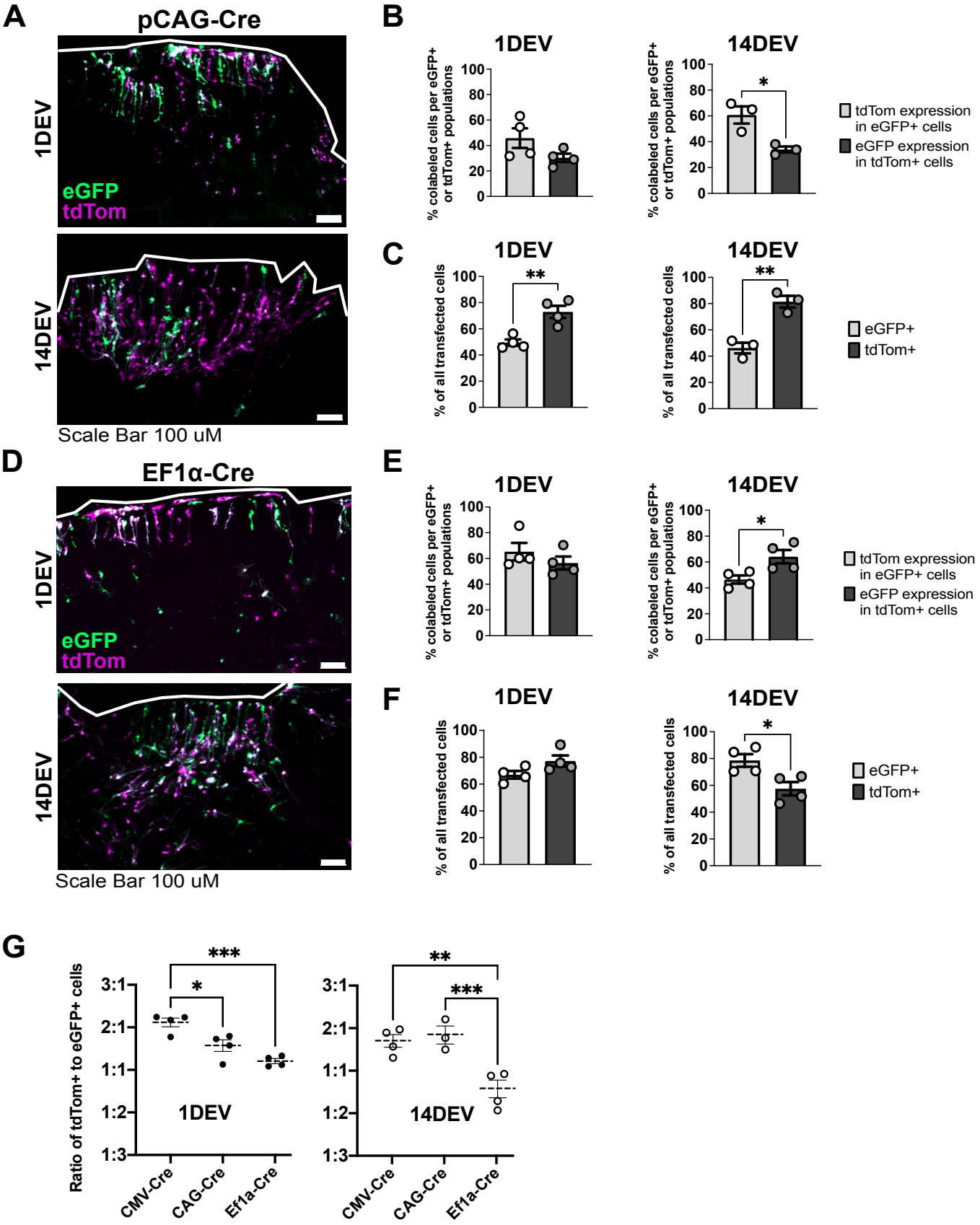
A
pCAG-Cre
1DEV
14DEV
eGFP
tdTom
Scale Bar 100 uM
B
1DEV
14DEV
% colabeled cells per eGFP+ or tdTom+ populations
tdTom expression in eGFP+ cells
eGFP expression in tdTom+ cells
C
% of all transfected cells
eGFP+
tdTom+
D
EF1α-Cre
Scale Bar 100 uM
E
F
G
Ratio of tdTom+ to eGFP+ cells
CMV-Cre
CAG-Cre
Ef1a-Cre